Research in Astron. Astrophys. **2009** Vol. **9** No. **XX**, 000–000
http://www.raa-journal.org *http://www.iop.org/journals/raa*

***R**esearch in*
***A**stronomy and*
***A**strophysics*

Multicolor Photometry of the Galaxy Cluster A98: Substructures and Star Formation Properties

L. Zhang[1], Q.-R. Yuan[1], X. Zhou[2], Z.-J. Jiang[2], Y.-B. Yang[2], J. Ma[2], J.-H. Wu[2] and Z.-Y. Wu[2]

[1] Department of Physics, Nanjing Normal University, Wenyuan Road 3, Nanjing 210046, China; Email: *yuanqirong@njnu.edu.cn; lizhang722@163.com*
[2] National Astronomical Observatories, Chinese Academy of Sciences, Beijing 100012, China.

Abstract An optical photometric observation with the Beijing-Arizona-Taiwan-Connecticut (BATC) multicolor system is carried out for A98 ($z = 0.104$), a galaxy cluster with two large enhancements in X-ray surface brightness. The spectral energy distributions (SEDs) covering 15 intermediate bands are obtained for all sources detected down to $V \sim 20$ mag in a field of $58' \times 58'$. After the star-galaxy separation by the color-color diagrams, a photometric redshift technique is applied to the galaxy sample for further membership determination. The color-magnitude relation is taken as a further restriction of the early-type cluster galaxies. As a result, a list of 198 faint member galaxies is achieved. Based on newly generated sample of member galaxies, the dynamical substructures, A98N, A98S, and A98W, are investigated in detail. A separate galaxy group, A98X, is also found to the south of main concentration of A98, which is gravitationally unbound to A98. For 74 spectroscopically confirmed member galaxies, the environmental effect on the star formation histories is found. The bright galaxies in the core region are found to have shorter time scales of star formation, longer mean stellar ages, and higher metallicities of interstellar medium, which can be interpreted in the context of hierarchical cosmological scenario.

Key words: galaxies: clusters: individual (A98) — galaxies: distances and redshifts — galaxies: kinematics and dynamics — galaxies: evolution — methods: data analysis

1 INTRODUCTION

Following the hierarchical scenario of structure formation, massive clusters form through episodic mergers of subunits, such as groups and poor clusters, and through the continuous accretion of field galaxies along the filaments (Zeldovich et al.1982; West et al.1991, 1995; Colberg et al.2000). Both the X-ray and optical surveys have revealed a significant level of substructure in rich galaxy clusters (Rhee et al. 1991; Forman & Jones 1982; Beers et al. 1991; Sarazin et al. 1992; Henry & Briel 1993; Burns et al. 1994). Numerical simulation of the evolution of galaxy clusters indicates that at least 50% of apparently relaxed clusters contain significant substructures (Salvador-Sole et al.1993). The dynamics of these "lumpy" clusters thus provides a means for exploring cluster evolution, which may shed light on the theories of large-scale structure formation (Kauffmann et al. 1999).

A98 is a good example of clusters with multiple components. It is a rich (R=3), quite distant ($z = 0.1042$, D=5) cluster (Abell et al. 1989) without the large cD galaxy at its center (the Bautz-Morgan type -BM:II-III). It was first selected optically by Abell (1958), and was regarded as a single galaxy cluster

before the launch of the *Einstein* Observatory (Duus & Newell 1977). The X-ray surface brightness distribution of A98 exhibits two large enhancements which were considered to be associated with the north and south components (Forman et al. 1981; Henry et al. 1981; Jones & Forman 1999). From then, A98 was extensively studied as a typical double cluster. Dressler (1978a; 1978b) analyzed the galaxy distribution of A98, and suggested that it consists of two subclusters, namely the south (A98S) and the north (A98N) ones. The radial velocities for galaxies in A98 were discussed by many authors (Faber & Dressler 1977; Dressler 1978b; Beers et al. 1982; Zabludoff et al. 1990). However, the number of spectroscopically confirmed member galaxies in A98 in previous studies is very limited. Based on only 24 member galaxies, Beers, Geller, & Huchra (1982, hereafter BGH) estimated the virial masses, mass to luminosity ratios of A98N and A98S. By using the two-body model, they further calculated the probability of gravitational binding, and derived that the two subclusters would merge in another 3 billion years. Krempeć-Krygier & Krygier (1995, hereafter KK95) studied the dynamics of A98 on the basis of only 29 cluster members. As a rich cluster containing wide-angle tailed (WAT) radio galaxies, A98 is included in the sample of WAT-containing clusters in Pinkney et al. (2000, hereafter PBLGH). The redshifts of some galaxies in the A98 region were obtained in that paper, but they did not investigate the dynamics of A98 in detail.

Substructures in the optical surface density and radial velocity are the typical signatures that allow to identify merging clusters. In this paper, we collect 74 cluster galaxies with known spectroscopic redshifts from literature, and investigate the dynamical substructures in A98. For a better understanding of dynamics of A98, the faint member galaxies ($18.0 < m_V < 20.0$) should be taken into account. This paper will present a multicolor photometry of the galaxies in A98 with the Beijing-Arizona-Taiwan-Connecticut (BATC) system. Based on the spectral energy distributions (SEDs) of faint galaxies, we try to supplement a large number of new member galaxies by applying the photometric redshift technique. The enlarged data set may verify the spatial distribution and dynamical properties of A98 to an unprecedented depth. Additionally, the star formation histories of the bright member galaxies may help us to understand the evolution of A98.

This paper is organized as follows: In section2, we present the BATC multicolor photometric observations and data reduction. In section 3, we analyze the galaxies with known spectroscopic redshifts in the A98 field, and distinguish a new galaxy group at $z = 0.12$ from the main concentration of A98. Section 4 presents the SED selection of faint member galaxies of A98. In section 5, the dynamical substructures and star formation properties are investigated on the basis of the sample of spectroscopically confirmed members and the enlarged sample of member galaxies. Finally, we summarize our work in section 6. Throughout this paper we assume the cosmological parameters $H_0 = 70 \mathrm{kms}^{-1}\mathrm{Mpc}^{-1}$, $\Omega_m = 0.3$ and $\Omega_\Lambda = 0.7$.

2 OBSERVATION AND DATA REDUCTION

The BATC multicolor photometric survey is designed to obtain the optical SED information of the faint objects without spectroscopic observation using the 60/90 cm f/3 Schmidt telescope of the National Astronomical Observatories, Chinese Academy of Sciences (NAOC), located at Xinglong site with an altitude of 900m. Before October 2006, an old Ford CCD camera with a format of 2048×2048 was mounted at the main focus of the telescope. The field of view was 58'×58', with a scale of 1."7 pixel^{-1}. For pursuing a better spatial resolution and a higher sensitivity in blue bands, a new E2V 4096 × 4096 CCD camera was equipped. The field of view becomes larger (92' × 92') with a spatial scale of 1."35 pixel^{-1}. The pixel sizes for the old and new CCD cameras are $15\mu m$ and $12\mu m$, respectively, and the pixel size ratio is exactly 5:4. The newly equipped CCD camera has a high quantum efficiency of 92.2% at 4000 Å. The BATC filter system contains 15 intermediate-band filters covering the wavelength range from 3000 to 10000Å. These filters were especially designed to avoid bright night sky emission lines (Fan et al. 1996). The transmission curves can be found in Yuan et al. (2003) and Xia et al.(2002).

From 1996 to 2006, we accumulated 37 hours in only 12 bands, from d to p, with the old CCD camera. In recent two years the exposures in a,b,c filters were completed with the new CCD camera. The total exposure time reaches more than 42 hours (see the observational statistics in Table 1). With an

Table 1 Parameters of the BATC filters and the observational statistics of A98

No.	Filter name	λ_c^a (Å)	FWHM (Å)	Exposure (second)	Number of Images	Seeing^b (arcsec)	Objects Detected	Completeness magnitude
1	a	3360	222	10800	9	4.23	5107	21.0
2	b	3890	291	3600	3	3.41	6860	20.5
3	c	4210	309	5400	6	3.50	6900	20.5
4	d	4550	332	22366	19	4.19	5753	20.5
5	e	4920	374	12000	10	3.79	6643	20.5
6	f	5270	344	12000	10	4.95	7977	20.0
7	g	5795	289	7200	6	4.27	8122	20.0
8	h	6075	308	6000	5	4.41	8125	19.5
9	i	6660	491	6000	9	4.05	8108	19.5
10	j	7050	238	6000	5	7.53	7503	19.5
11	k	7490	192	7200	6	3.86	8010	19.0
12	m	8020	255	10800	9	4.12	8119	19.0
13	n	8480	167	10800	9	4.38	7928	19.0
14	o	9190	247	15000	13	3.74	8106	18.5
15	p	9745	275	20400	17	4.93	7609	18.5

Notes: ^{a} Central wavelengths of the filters; ^{b} This column lists the seeings of the combined images.

automatic data-processing software, PIPELINE I (Fan et al. 1996), we carried out the standard procedures of bias subtraction, flat-field correction, and position calibration. The technique of integral pixel shifting is used in the image combination during which the cosmic rays and bad pixels were removed by comparing multiple images.

For detecting and measuring the flux of sources within a given aperture in the BATC images, we use a photometry package, PIPELINE II, developed on the basis of DAOPHOT kernel (Zhou et al. 2003a), to perform aperture photometry. An object is considered to be detected if its signal to noise ratio is larger than the threshold 3.5 σ in i, j, and k bands. Thanks to the pixel size ratio between the old and new CCDs is 5:4, we adopt a radius of 4 pixels as the photometric aperture for the images in 12 bands (from d to p), and a radius of 5 pixels for the images in other three bands (from a to c). The flux calibration in the h band is performed using the Oke-Gunn primary flux standard star HD 19445, HD 84937, BD+26 2606, and BD+17 4708 (Gunn & Stryker 1983). To achieve the *relative* SEDs of the sources detected by the BATC system, Zhou et al. (1999) developed a method of model calibration on the basis of the stellar SED library. No calibration images of the standard stars are needed during the flux calibration. Using this model calibration method, as a result, the SEDs of about 9000 sources have been obtained for further analysis.

The magnitudes within a fixed photometric aperture is somewhat different from the total magnitudes of galaxies given in some catalogs. For assessing the measurement errors at specified magnitudes, we separate stars into different bins of magnitudes with an interval of 0.5 mag, and we find that magnitude error in each filter are larger at fainter depths. A typical error is less than 0.02 mag for the stars brighter than 16.5 mag, and about 0.05 mag for the stars with V $\sim$ 18.5 mag.

3 DISCOVERY OF A NEW GALAXY GROUP 'A98X'

3.1 Distribution of spectroscopic redshifts

For studying the dynamics of the galaxy cluster A98, 122 galaxies with known spectroscopic redshifts (z_{sp}) in the $58' \times 58'$ field centered at A98 are extracted from NASA/IPAC Extragalactic Database (NED). Most of the spectroscopic data were contributed by Struble & Rood (1999) who present a compilation of the redshifts for 1572 rich clusters in Abell, Corwin & Olowin (1989). Fig. 1a shows the distribution of spectroscopic redshifts of these bright galaxies. The highest peak, centered at $z_{sp} \sim 0.104$, is isolated and less contaminated. So it is unambiguous to regard the 74 galaxies with $0.095 < z_{sp} < 0.115$

Table 2 Catalog of spectroscopically confirmed member galaxies in A98

No.	R.A.	Decl	z_{sp}	Ref.	No.	R.A.	Decl	z_{sp}	Ref.
1	0 45 33.0	20 15 09	0.1003	1	38	0 46 24.7	20 37 19	0.1028	2
2	0 45 40.2	20 15 58	0.0999	1	39	0 46 25.8	20 29 06	0.1094	2
3	0 45 41.3	20 31 01	0.1030	1	40	0 46 25.9	20 27 33	0.1041	3
4	0 45 41.3	20 28 02	0.0961	1	41	0 46 26.8	20 36 52	0.0995	1
5	0 45 45.5	20 26 17	0.1045	2	42	0 46 28.5	20 23 49	0.1013	4
6	0 45 46.9	20 26 57	0.1043	3	43	0 46 29.3	20 28 05	0.1032	3
7	0 45 48.1	20 27 36	0.1034	2	44	0 46 29.5	20 33 19	0.1045	3
8	0 45 48.6	20 26 06	0.1039	1	45	0 46 29.8	20 38 58	0.1088	3
9	0 45 50.1	20 29 10	0.1012	1	46	0 46 29.9	20 34 28	0.0978	1
10	0 45 50.4	20 27 49	0.1037	4	47	0 46 30.1	20 36 49	0.0980	3
11	0 45 50.5	20 29 07	0.1033	1	48	0 46 31.1	20 31 44	0.1034	1
12	0 45 57.4	20 36 56	0.1013	1	49	0 46 31.8	20 28 11	0.1082	2
13	0 45 59.3	20 23 50	0.1058	1	50	0 46 32.0	20 28 27	0.1048	1
14	0 46 02.1	20 30 51	0.0996	1	51	0 46 32.1	20 43 06	0.1046	1
15	0 46 02.2	20 30 30	0.1060	1	52	0 46 32.5	20 28 24	0.1060	1
16	0 46 04.0	20 34 51	0.1005	3	53	0 46 33.9	20 23 55	0.1091	1
17	0 46 04.5	20 36 45	0.1044	4	54	0 46 35.2	20 30 11	0.1041	1
18	0 46 04.7	20 28 28	0.1054	1	55	0 46 35.2	20 20 32	0.1024	1
19	0 46 07.4	20 28 49	0.1059	1	56	0 46 35.6	20 29 43	0.1067	3
20	0 46 07.8	20 38 47	0.1060	1	57	0 46 36.2	20 28 27	0.1073	3
21	0 46 08.0	20 40 45	0.1019	2	58	0 46 37.0	20 26 07	0.1023	4
22	0 46 08.4	20 28 51	0.1013	3	59	0 46 38.1	20 28 41	0.1033	1
23	0 46 14.7	20 23 43	0.1034	1	60	0 46 38.5	20 22 54	0.1037	4
24	0 46 15.5	20 33 20	0.1001	1	61	0 46 43.2	20 36 05	0.1045	3
25	0 46 15.8	20 32 06	0.1024	1	62	0 46 48.0	20 30 55	0.1036	1
26	0 46 15.8	20 38 09	0.1072	3	63	0 46 49.2	20 27 24	0.0978	1
27	0 46 15.8	20 39 08	0.1075	2	64	0 46 50.0	20 27 08	0.1055	1
28	0 46 16.0	20 30 19	0.1017	2	65	0 46 51.5	20 30 23	0.1019	1
29	0 46 18.5	20 33 14	0.1051	1	66	0 46 51.8	20 30 43	0.1062	1
30	0 46 19.2	20 28 12	0.1016	1	67	0 46 52.6	20 25 23	0.1086	1
31	0 46 19.3	20 29 42	0.1098	2	68	0 46 52.8	20 41 00	0.1051	3
32	0 46 20.3	20 28 59	0.1014	1	69	0 46 56.5	20 27 05	0.1009	1
33	0 46 20.6	20 29 08	0.1032	1	70	0 46 56.9	20 40 25	0.1031	2
34	0 46 21.6	20 42 31	0.1046	1	71	0 47 01.7	20 23 18	0.1049	1
35	0 46 21.9	20 29 05	0.1116	3	72	0 47 09.4	20 29 17	0.1051	1
36	0 46 23.8	20 30 01	0.0998	2	73	0 47 13.0	20 29 41	0.1069	1
37	0 46 24.6	20 30 06	0.1043	3	74	0 47 18.0	20 22 01	0.1049	1

Notes: References: (1)Pinkney et al. (2000); (2) Zabludoff et al. (1990); (3) Beers et al. (1982); (4) Bettoni et al. (2006).

as the spectroscopically confirmed member galaxies in A98, and we refer to these member galaxies as 'sample I'. Table 2 lists the information of the position and spectroscopic redshift of these 74 galaxies.

To quantify the velocity distribution of member galaxies, we firstly convert the redshifts into true cosmological velocities by $v = c[(1+z_{sp})^2-1]/[(1+z_{sp})^2+1]$, where c is the light speed. Then, we use the ROSTAT software (Beers, Flynn, & Gebhardt 1990) to calculate two resistant and robust estimators analogous to the velocity mean and standard deviation, namely, the biweight location (C_{BI}) and scale (S_{BI}). For these 74 member galaxies, we achieve $C_{BI} = 29505 \pm 94$ km s^{-1}and $S_{BI} = 809 \pm 77$ km s^{-1}. Fig. 1b shows the distribution of the line-of-sight velocities for these 74 galaxies. Taking a cosmological correction factor of $(1 + z)^{-1}$ into account, the velocity dispersion of A98 should be 732 ± 70 km s^{-1}.

Our sample of member galaxies is much larger than the ones in BGH and KK95. Based on only 29 member galaxies, KK95 derived a mean velocity of 29757 km s^{-1}and a velocity dispersion of 859 km s^{-1}. Using 69 member galaxies in A98, PBLGH derived the mean velocity of 31085 ± 96 km s^{-1}and the velocity dispersion of 797 ± 73 km s^{-1}. Their values are larger than our estimates due to the contamination of the galaxy group at $z = 0.120$, which will be discussed in the next subsection.

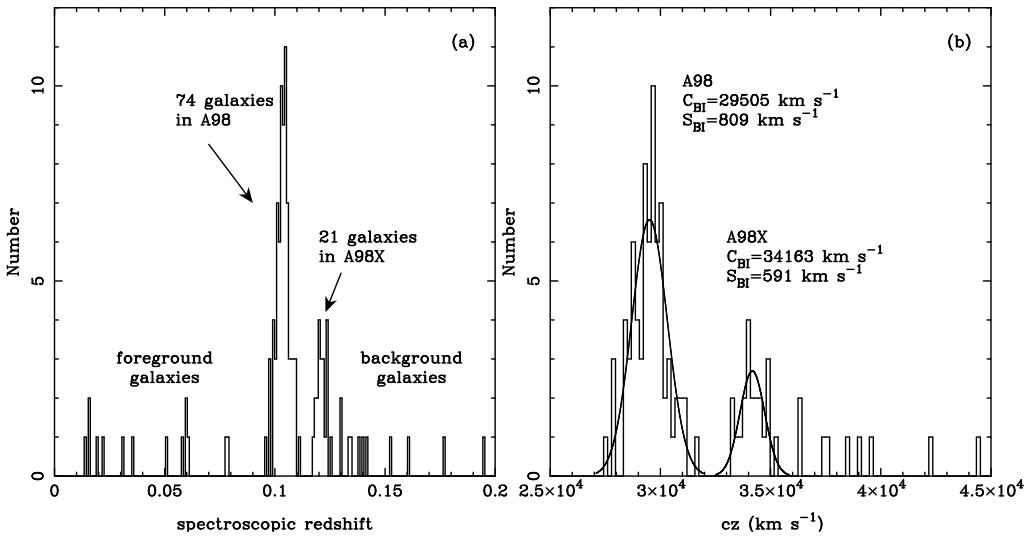

Fig. 1 Left: Distribution of spectroscopic redshifts for 122 known galaxies in the A98 region. The bin size is 0.00125. Right: Distribution of radial velocities for the galaxies in A98 and A98X, with a Gaussian fitting superposed on each component.

3.2 The south clump 'A98X' at $z = 0.120$

It is interesting to find in Fig. 1 that there are 21 galaxies with the redshifts between 0.115 and 0.128. For this velocity concentration, we obtain the biweight location of $C_{BI} = 34163 \pm 133$ km s^{-1}and the biweight scale of $S_{BI} = 591 \pm 76$ km s^{-1}. Considering the cosmological correction, the velocity dispersion of this peak is 528 ± 68 km s^{-1}. The separation between these two velocity peaks is about 4658 ± 163 km s^{-1}.

The left panel of Fig. 2 shows the spatial distribution for 74 member galaxies(denoted by asterisks) and 21 galaxies with the redshifts between 0.115 and 0.128 (denoted by open triangles), with respect to the NED-given central position of A98 ($00^h46^m26.^s6$, $+20°29'23"$; J2000.0). We superpose the contour maps of surface density that has been smoothed by a Gaussian window of $\sigma = 1.'6$. The contour map shows that these 21 galaxies with $z_{sp} \sim 0.120$ belong to a separate clump, about 15' south to the main concentration. As the separation between the two peaks is very remarkable, we refer to the south clump as 'A98X'.

To show the prominence of the clump A98X in both the velocity space and the projected map, we make use of the κ-test (Colless & Dunn 1996) for the A98/A98X system as a whole. The statistic κ_n is defined to quantify the local deviation on the scale of groups of n nearest neighbors. A larger κ_n indicates a greater probability that the local velocity distribution differs from the overall velocity distribution. The probability $P(\kappa_n > \kappa_n^{obs})$ can be calculated by Monto Carlo simulations with random shuffling velocities. When the scale of the nearest neighbors n varies from 3 to 10, the probability $P(\kappa_n > \kappa_n^{obs})$ is nearly zero, which means the substructure appears very obvious at different scales. The bubble plot at $n = 6$ is given in the right panel of Fig. 2. Since the bubble size is proportional to $-\log[P_{KS}(D > D_{obs})]$, the clustering of larger bubbles at (1.'55,-14.'43) can trace the significant substructure, which corresponds to the galaxy group 'A98X' centered at ($0^h46^m33.^s2$, $20°14'57"$; J2000.0).

We fail to find any clusters and/or groups of galaxies from literature and existing catalogs of galaxy clusters around the position of the clump A98X. This concentration has not been mentioned in any previous investigations. An interesting question is whether the clump A98X is just a subcluster of A98

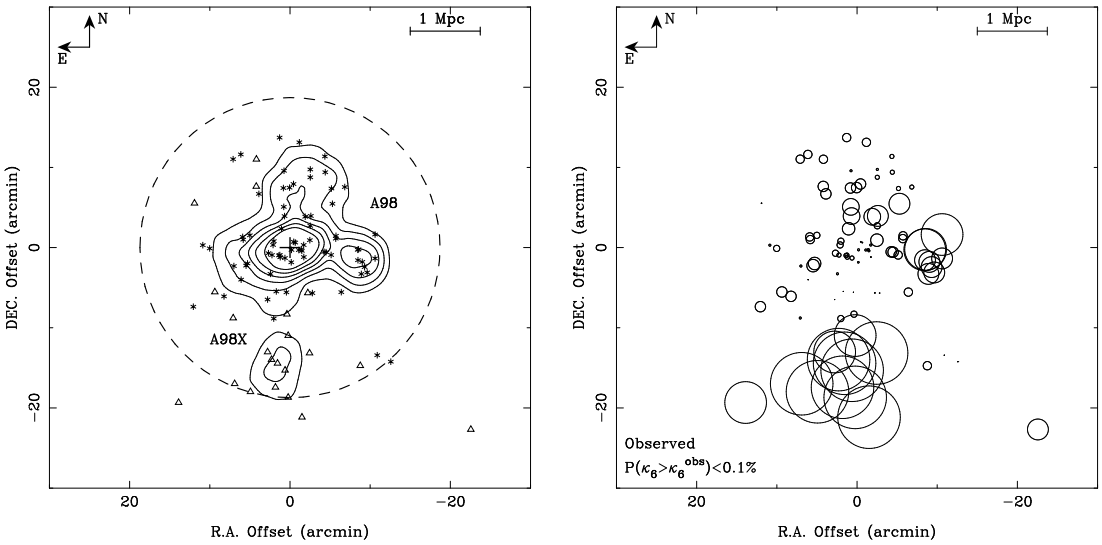

Fig. 2 Left: Spatial distribution for 95 galaxies in A98 (denoted by asterisks) and A98X (denoted by triangles), superposed by the contour map of surface density where the smoothing Gaussian window with $\sigma = 1.'6$ is used. The contour levels are 0.09,0.15,0.21,0.27,0.33,0.39 $arcmin^{-2}$, respectively. The dashed circle means a typical region of rich clusters with the Abell radius of $1.5h^{-1}$ Mpc; Right: Bubble plot for the 95 galaxies in the A98 and A98X components.

or a newly-detected cluster/group of galaxies. To answer this question, it is necessary to verify whether A98X is gravitationally bound to the A98 cluster or not.

3.3 The Application of Gravitational Binding Criterion

The masses of the main concentration of A98 and the clump A98X can be estimated by applying virial theorem. Assuming that each cluster is bound and the galaxy orbits are random, the virial mass (M_{vt}) can be derived from the following standard formula (Geller & Peebles 1973; Oegerle & Hill 1994):

$$M_{vt} = \frac{3\pi}{G}\sigma_r^2 D N_p \left(\sum_{i>j}^{N}\frac{1}{\theta_{ij}}\right)^{-1}, \quad (1)$$

where σ_r is the line-of-sight velocity dispersion, D is the cosmological distance of the cluster, $N_p = N(N-1)/2$ is the number of galaxy pairs, and θ_{ij} is the angular separation between the galaxies i and j. The virial masses of $9.12\times10^{14}M_\odot$ and $7.98\times10^{14}M_\odot$ are derived for A98 and A98X, respectively. Then we specify the limits of the bound solutions by using Newtonian criterion of gravitational binding (Beers et al. 1982):

$$V_r^2 R_p \leq 2GM\sin^2\alpha\cos\alpha, \quad (2)$$

where V_r is the relative velocity along the line of sight, R_p is the projected separation, M is the total mass of the two clusters, and α is the angle between the plane of the sky and the line connecting the two clusters. The projected separation of A98 and A98X is $R_p = 1.78$ Mpc, and the actual observed $V_r \sim 4200 \pm 163 \mathrm{km}s^{-1}$ in the rest frame of A98. The resulting constraints on V_r for bound orbits are shown in Fig. 3, as a function of the projection angle, α. The solid curve in this plot separates the regions of bound and unbound. As the figure shows, the maximum V_r value for the bound solution is ~ 1800 km s^{-1}, which is obviously much lower than the observed $V_r \sim 4200 \pm 163$ km s^{-1}. There is no doubt that the clump A98X containing 21 galaxies is gravitationally unbound to the cluster A98.

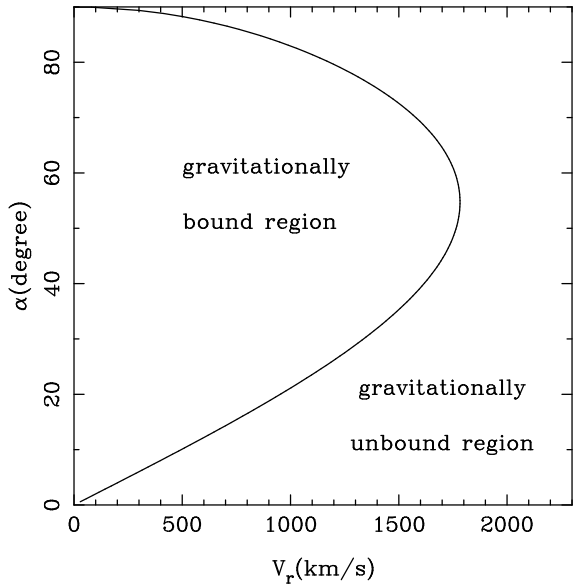

Fig. 3 Projection angle α as a function of radial velocity V_r given by the total mass $1.71 \times 10^{15} M_{\odot}$. The solid curve separates the bound and unbound regions.

Our conclusion is that the A98X is a separate group of galaxies. In our following dynamical analysis of A98, this galaxy group will be excluded.

It should be noted that the main concentration of A98 is not a well virialized system which contains more than two subclumps (see section 5). It might be arbitrary to derive the mass of main concentration via the virial theorem. However, we believe that the probable bias in our mass estimate is not significant enough to influence above conclusion.

4 SED SELECTION OF FAINT CLUSTER GALAXIES

4.1 Star-Galaxy Separation

For the galaxies with known spectroscopic redshifts given by the NED, we cross-identified with the BATC-detected sources. All the sources in the BATC catalog within the searching circle (defined by a radius of 5") centered on the NED-given galaxies were extracted. The identification is rather unambiguous. For the case of several counterparts within the searching area, we pick up the brighter BATC source as the right counterpart. As a result, 118 bright galaxies with known z_{sp} values are identified. The 15-band SEDs of these galaxies will be used to check the reliability of our photometric redshift technique.

For selecting the probable faint member galaxies from the remaining BATC sources, we firstly perform the star/galaxy separation. As shown in Yuan et al.(2001), the color-color diagram is a powerful tool of classification. Since the spectra of redshifted galaxies differ significantly from those of stars, different regions in the color-color diagram are occupied by different classes of objects. Fig. 4 shows two color-color diagrams used for our star-galaxy separation. The diagrams include the following categories of sources: (1) all types of stars in our SED template library (denoted by filled triangles), (2) morphologically various galaxies with template SEDs (denoted by open circles), (3) the spectroscopically confirmed member galaxies of A98 (denoted by crosses), and (4) all the remaining sources detected by the BATC photometry (denoted by dots). The filters a(3360Å),b(3890Å),h(6075Å), and p(9745Å) are used in the diagrams. It can be seen in Fig. 4 that the stars in the SED template library lie in a well-defined zone stretching from top left to bottom right, while the confirmed galaxies distribute just above the zone. Taking the dashed lines in Fig.4 as the boundaries of star-galaxy separation, we pick out the

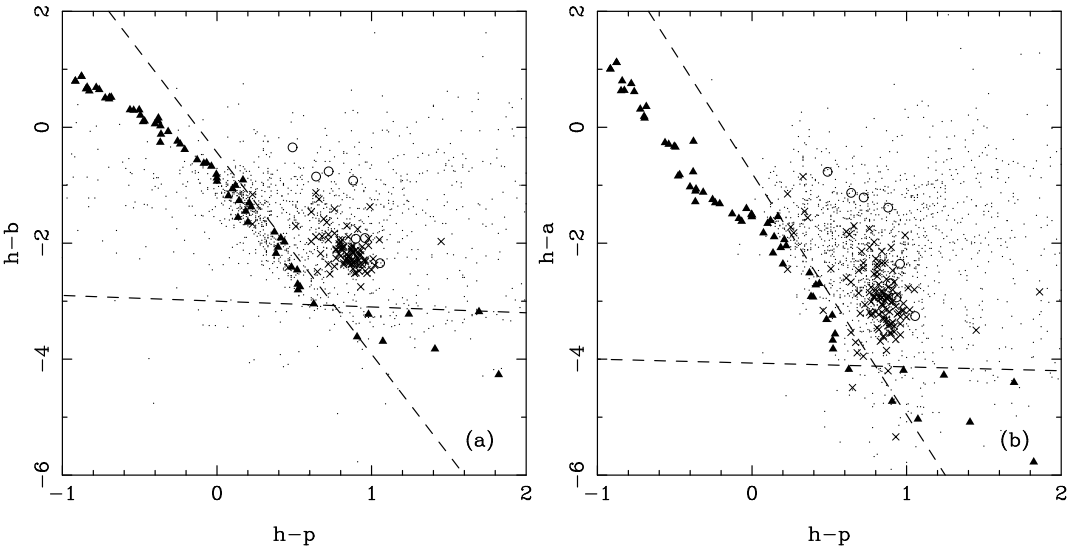

Fig. 4 Color-color diagrams used for star-galaxy separation (Asterisks for all types of stars in the SED template library, open circles for various galaxies with template SEDs, crosses for the confirmed galaxy, small dots for the detected sources). The dashed lines are taken as boundaries of separation.

galaxies simultaneously detected in at least 11 BATC bands. As a result, we obtained 1490 faint galaxies that are located within the boundries in both panels, to which we shall apply the photometric redshift technique.

4.2 Photometric Redshifts and Cluster Membership

The technique of photometric redshift can be used to estimate the redshifts of galaxies by using the SED information covered a wide range of wavelength instead of the spectroscopy. This technique is extensively applied to the multicolor photometric surveys for detecting the faint and distant galaxies (Pelló et al. 1999a, b; Bolzonella et al. 2000; Rowan-Robinson et al. 2008; Ilbert et al. 2009) and for selecting the cluster galaxies (Brunner & Lubin 2000; Finoguenov et al. 2007). For a given object, based on the standard SED-fitting code called HYPERZ (Bolzonella, Miralles, & Pelló 2000), the photometric redshift, z_{ph}, corresponds to the best fit (in the χ^2-sense) between its photometric SED and the template SED generated by convolving the galaxy spectra in template library with the transmission curves of BATC filters. Previous work has evaluated the accuracy of photometric redshift with the BATC multi-band data (Yuan et al. 2001, 2003; Zhou et al. 2003b; Yang et al. 2004). In our SED fitting, only the normal galaxies are taken into account in the reference templates. The dust extinction with a reddening law of the Milky Way (Allen 1976) is adopted, and A_V is allowed to be flexible in a range from 0.0 to 0.2, with a step of 0.02. The photometric redshift of a galaxy with the BATC SED is searched from 0.0 to 0.5, with a step of 0.005.

For the 118 galaxies with known spectroscopic redshifts, a comparison between the photometric redshifts z_{ph} and the spectroscopic redshifts z_{sp} is shown in Fig. 5. The solid line corresponds to $z_{ph} = z_{sp}$, and the dashed lines indicate an average redshift deviation of 0.023, and the error bar of z_{ph} corresponds to 68% confidence level in photometric redshift determination. It is obvious that our z_{ph} estimate is basically consistent with the spectroscopic redshift. For the 74 member galaxies in sample I, the biweight location (C_{BI}) and scale (S_{BI}) of the z_{ph} estimate are 0.097 and 0.008, respectively. There exists a slight systematic offset in the z_{ph} distribution, with respective to the z_{sp} distribution.

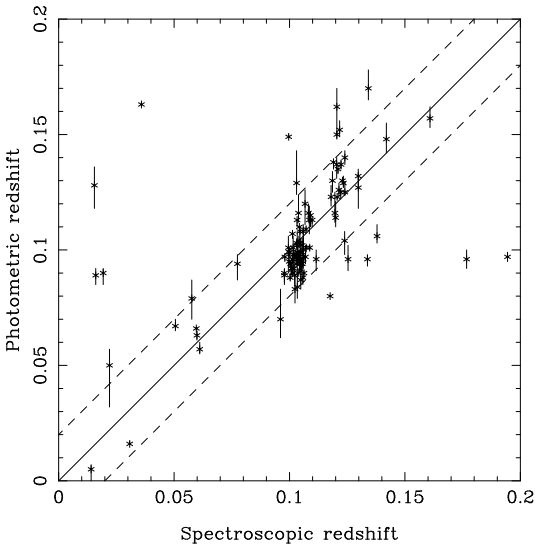

Fig. 5 Comparison between photometric redshift z_{ph} and spectroscopic redshift z_{sp} for 118 galaxies in the field of view. The solid line corresponds to $z_{ph} = z_{sp}$, and the dashed lines indicate an average deviation of 0.023.

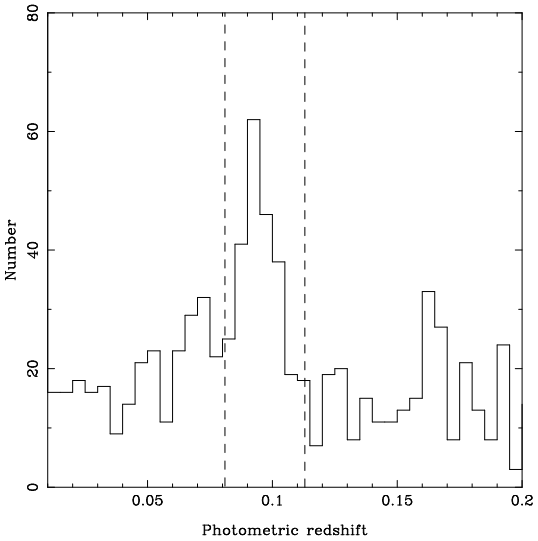

Fig. 6 Distribution of photometric redshifts for the galaxies ($z < 0.2$) . The dashed lines are plotted as the photometric redshift range of cluster member candidates.

Taking the selection criterium of 2σ clipping, 65 member galaxies (about 90 percent) are found to have their photometric redshifts in a range from 0.081 ($= 0.097 - 2 \times 0.008$) to 0.113 ($= 0.097 + 2 \times 0.008$). This z_{ph} region can be applied as a selection criterium in the following membership determination for the faint galaxies detected by the BATC multicolor photometry only.

Fig. 6 shows the histogram of photometric redshifts for faint galaxies with $z_{ph} < 0.2$ in the viewing field. The galaxies with $0.081 < z_{ph} < 0.113$ within one Abell radius ($1.5h^{-1}$Mpc), corresponding to 18.71 arcmin at $z = 0.104$, are selected as member candidates of A98. As a result, there are 198 faint member candidates, among which 137 galaxies are regarded as early-type galaxies and 61 galaxies are regarded as late-type galaxies by the SED-fitting procedure.

It is well known that there exists a correlation between the color and absolute magnitude for the early-type galaxies (C-M relation, see Bower et al. 1992), in the sense that the bright galaxies are redder, which can be used for verifying the membership selection of the early-type galaxies. For selecting the early-type galaxies, We take the morphological types of the best-fit SED templates. Fig. 7 presents the correlation between the color index $b - h$ and magnitude in h bandpass for 203 early-type member galaxies, including 66 early-type galaxies with known z_{sp} and 137 newly-selected early-type galaxies. The solid line denotes the linear fitting of the 66 spectroscopically confirmed member galaxies: $b - h = -0.10(\pm 0.04)h + 3.89(\pm 0.79)$, and the dashed lines represent 1 σ deviation. As shown in Fig. 7, most majority of the early-type candidates agree with the C-M relation derived by 66 bright early-type galaxies. There is no faint early-type candidates with the color $b-h$ beyond the 2 σ deviation of intercept. By combining the 198 newly-selected members and 74 spectroscopically confirmed member galaxies in sample I, we obtain an enlarged sample of 272 member galaxies, which is referred to as sample II.

Table 3 presents the catalog of SED information for the 198 newly selected members, as well as the celestial coordinate, photometric redshift, and morphological class of the best-fit template. The classification indices, T, ranging from 1 to 7, are defined to denote E, S0, Sa, Sb, Sc, Sd, and Im galaxies, respectively.

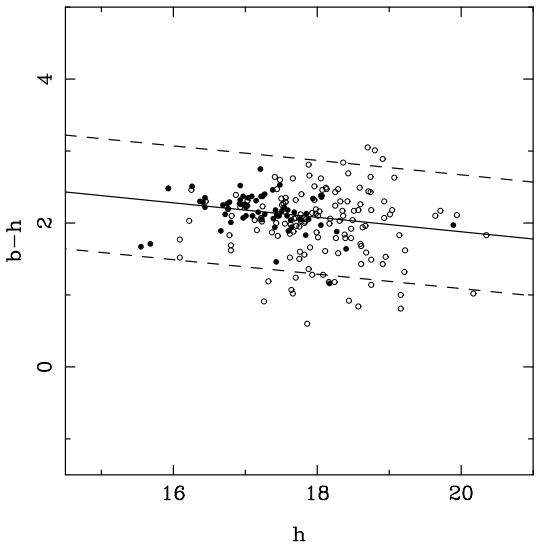

Fig. 7 Color-magnitude correlation for 203 early-type galaxies in A98. Filled circles denote 66 early-type member galaxies which have been spectroscopically confirmed, and open circles denote 137 newly-selected member galaxies. The solid line shows the linear fit for 66 bright galaxies, and the dashed lines correspond to 1 σ deviation.

5 THE PROPERTIES OF THE CLUSTER A98

5.1 Projected Distribution of Cluster Galaxies

Fig. 8 shows the projected position of the galaxies in samples I and II, superposed with the contour maps of surface density where the smoothing Gaussian window of $\sigma = 1.'6$ is used. 74 member galaxies with known spectroscopic redshifts are denoted by filled circles and 198 photometrically selected galaxies are denoted by open circles. Two X-ray peaks given in Forman et al.(1981) are also marked with filled triangles. Fig.8a shows that the 74 bright member galaxies of A98 seem to deviate from spherically symmetric distribution. The contour map of surface density appears elongated in the north-south direction. Two X-ray peaks are found to be associated with the surface density substructures A98N and A98S. Previous spectroscopy shows that the subcluster A98N is much poorer than the main concentration A98S, which is remarkable in Fig. 8a. Our BATC multicolor photometry facilitates the finding of large number of faint member galaxies around the northern subcluster A98N, which makes the northern substructure in surface density more remarkable (see Fig. 8b).

What we should keep in mind is that the surface density of A98N is still lower than that of A98S, even after we take all the faint member galaxies into account. However, the northern subcluster A98N is brighter than the southern A98S in the X-ray emission. Forman et al. (1981) reported that the flux ratio between A98N and A98S is about 3:2. Henry et al. (1981) derived a ratio of X-ray luminosity between A98N and A98S of 1.3:1. Considering the contribution in X-ray surface brightness of the central galaxy 0043+2020, KK95 fitted with the β model, and obtained a lower X-ray luminosity ratio of 1.1:1.

Apart from the northern subcluster A98N, a western subcluster can be seen in Fig. 8, at about 12 arcmin west of A98S. This subcluster has not been mentioned before, and we refer to it as A98W. After adding 198 photometrically selected galaxies, Fig. 8b shows that A98N appears more significant and the western clump A98W still exists. In general, the projected position distribution of the galaxies in sample II is consistent with that of the bright galaxies in sample I.

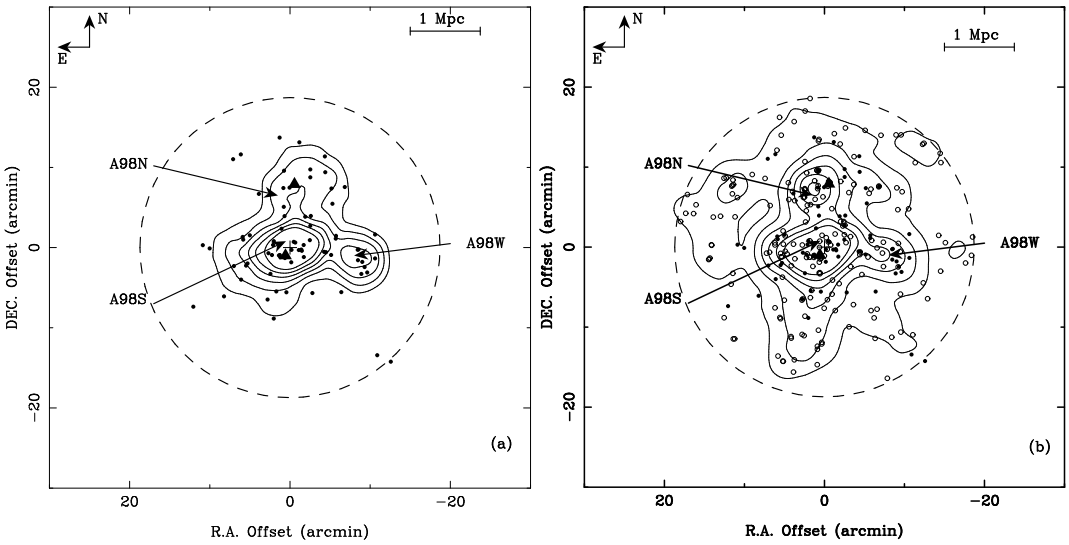

Fig. 8 Left (a): The positions of 74 spectroscopic member galaxies of A98 in sample I. The surface density is smoothed with a Gaussian window of $\sigma = 1.'6$. Contour map is superposed with the surface density levels 0.09,0.15,0.21,0.27,0.33,0.39 arcmin^{-2}. The dashed circle means a typical region of rich clusters with the Abell radius of $1.5h^{-1}$ Mpc. Two X-ray peaks are marked with filled triangles. Right (b): Position distribution of the 272 member galaxies in sample II, including 74 spectroscopically confirmed member galaxies (filled circles) and 198 newly-selected galaxies (open circles). The contour map of the surface density for these galaxies are also given with contour levels 0.13,0.28,0.43,0.58,0.73,0.88 arcmin^{-2}.

5.2 Localized Velocity Structure

However, the clumps mentioned above might be the enhancement simply due to projection effect. If a cluster merger occurs along the direction with a definite projection angle, say $\alpha > 20^{\circ}$, with respective to the plane of sky, the substructures can be detected by mapping the localized variation in velocity distribution (Colless & Dunn 1996). The κ-test defines a test statistic κ_n to characterize the local deviation on the scale of groups of n nearest neighbors.

For detecting the substructures in A98, we perform the κ-test for the galaxies in samples I and II. For sample I, there is no significant substructure detected in the localized velocity. We performed 10^3 simulations to estimate probability $P(\kappa_n > \kappa_n^{obs})$ in all cases. The probability $P(\kappa_n > \kappa_n^{obs})$ is found to be more than 5% in a wide range of neighbor sizes, which means that no substructure is detected at 2σ significance. Table 4 gives the result of our κ-test for the galaxies in sample I. However, for the enlarged sample of 272 member galaxies, the probability of substructure detection is greater. Considering the larger relative error in photometric redshift determination, the probability estimate of sample II might be untrue.

Table 4 Result of κ-Test for 74 spectroscopically confirmed member galaxies

Neighbor size n	3	4	5	6	7	8	9
$P(\kappa_n > \kappa_n^{\rm obs})$	11.4.2%	5.3%	9.2%	14.4%	16.6%	24.9%	40.6%

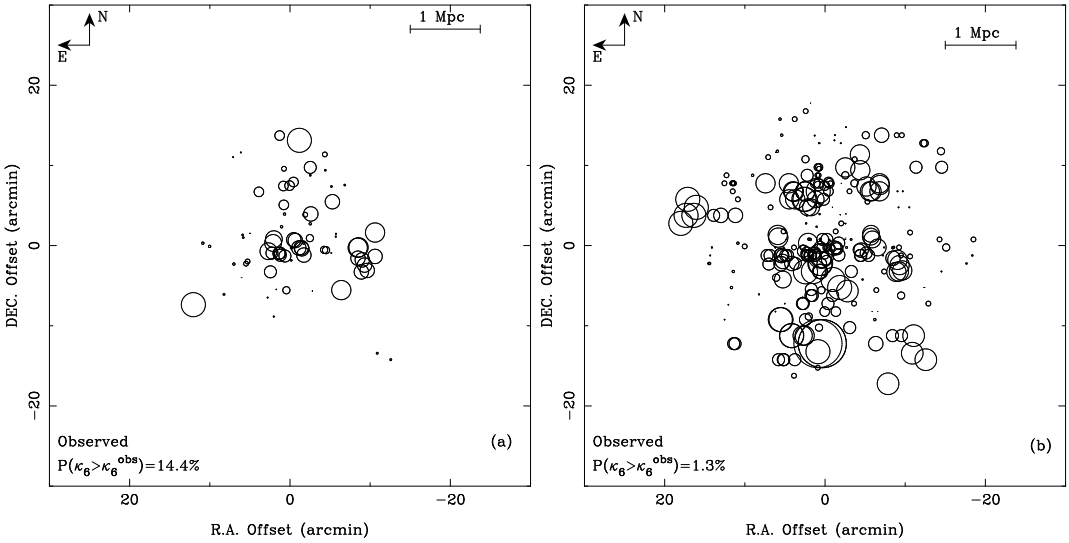

Fig. 9 (a)Bubble plot for 74 spectroscopic member galaxies of A98. It shows the localized variation for groups of the six nearest neighbors. (b)Bubble plot for all the 272 member galaxies of A98. The same group size as Fig.(a) is used to characterize the localized variation.

Bubble plots in Fig. 9 show the localized velocity variation for sample I and sample II, using 6 nearest neighbors. The bubble size for each galaxy is proportional to $-log[P_{KS}(D > D_{obs})]$. For the galaxies in sample I (see Fig. 9a), there are indeed bunches of bubbles at the positions of subcluster A98S and A98W, though the bubble sizes are not very large. A close comparison between Fig. 8a and Fig. 9a indicates that A98S and A98W are not simply due to projection effect, they are most likely to be real substructures. On the other hand, no bubble clustering is found for the northern subcluster A98N. It seems to support the two-body model that we are looking at a cluster merger between A98N and A98S occurred largely in the plane of the sky, which is consistent with the small projection angle derived in KK95.

For the galaxies in sample II (see Fig. 9b), the clustering of bubbles at A98N is enhanced. Taking the faint member galaxies into account, the localized velocity variation between A98S and A98N appears more remarkable. Within the central regions of A98N and A98S, defined by the contour curve at 0.58 arcmin^{-2} in Fig. 8b, there are 28 and 73 galaxies, respectively. For the 28 galaxies in A98N, the biweight location is 27029 ± 335 km s^{-1}, However, for the 73 galaxies in A98S, we obtain a higher biweight location, 28721 ± 207 km s^{-1}. The difference in radial velocity between A98N and A98S is about 1692 ± 394 km s^{-1}, which is larger than the typical velocity dispersion of a rich cluster. Fig. 10 gives the distributions of radial velocities for these galaxies. The large velocity difference seems to be a challenge for the bound system. It is noteworthy that the photometric redshifts for the faint member galaxies have a lower precision, and it is necessary to verify the inertal dynamics between A98N and A98S by the follow-up deep spectroscopic observation. There are only 6 and 27 galaxies with known z_{sp} values within the central regions of A98N and A98S, respectively, for which the velocity distributions are shown in the shadowed histograms in Fig. 10. For the spectroscopic subsamples in A98N and A98S central regions, the biweight locations are 28943 and 29609 km s^{-1}, respectively. The velocity difference becomes about 666 km s^{-1}, much smaller than the value of enlarged samples, which supports the gravitationally bound nature of these two subclusters.

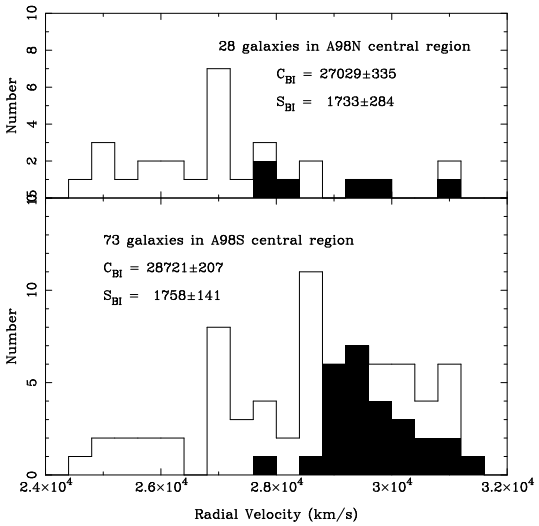

Fig. 10 Velocity distribution of the galaxies in the central regions of A98N and A98S, defined by the contour curve at 0.58 arcmin^{-2} in Fig. 8b. The velocity distributions of the galaxies in spectroscopic subsamples are shown by the shadowed histograms.

5.3 Star Formation Properties

Undoubtedly, the star formation histories of the member galaxies may shed some light on the evolution of their host cluster. With the evolutionary synthesis model, PEGASE (version 2.0, Fioc & Rocca-Volmerange 1997; 1999), we study the star formation properties of A98. Assuming a Salpeter (1955) initial mass function (IMF) and a star formation rate (SFR) in exponentially decreasing form, $SFR(t) \propto e^{-t/\tau}$, where the time scale τ ranges from 0.5 to 30.0 Gyr. In order to avoid the degeneracy between age and metallicity in the model, we adopt the same age of 12.2 Gyr, responding to the age of first generation stars at $z = 0.104$, for all member galaxies in A98. A zero initial metallicity of interstellar medium (ISM) is taken. As a result, a series of rest-frame modelled spectra with various star formation histories are generated by running the PEGASE code, and then they are redshifted to the observer frame for a given spectroscopic redshift. Convolved with the transmission functions of all the BATC filters, the template SED library for the BATC multicolor photometric system (i.e., relative apparent magnitudes at 15 BATC fileters) can be obtained.

Based on the template SED library, we search for the best fit (in the χ^2 sense) of the observed SEDs of 74 member galaxies with known spectroscopic redshifts. The SFR time scale (τ), mean ISM metallicity (Z_{ISM}), and mean stellar age ($t_\star$) can be derived for each bright galaxy. Fig. 11 presents the star formation properties as a function of the local surface density, Σ, which is defined by the number of galaxies within an area with a radius of 2.5 arcmin. It is clear in Fig. 11 that the star formation property of the member galaxies in A98 are found to be dependent upon the local density. Panel (a) shows that the galaxies in the outer region are likely to have a longer SFR time scales than those in the core region. Considering that the late-type galaxies tend to have longer time scales of star formation, our result is consistent with the morphology-density relation first pointed out by Dressler (1980), which can be well explained in the context of hierarchical cosmological scenario (Poggianti 2004). As shown in the panels (c) and (d), the outlier member galaxies are likely to possess younger stellar population, which results in a smaller mean stellar age weighted by either mass or light.

Fig. 11b gives the variation of the mean ISM metallicities with their local densities. The outlier galaxies have higher probability to have a lower mean ISM metallicity. It is regarded that the galaxies in the core region tend to be more massive and luminous. The underlying physical correlation that can

interpret Fig. 11b is the luminosity-metallicity relation (Lequeux et al. 1979; Melbourne & Salzer 2002) and the mass-metallicity relation (e.g., Garnett & Shields 1987; Tremonti et al. 2004). Fig. 12 gives the SFR time scales τ and the mean ISM metallicities as the functions of the magnitude in h band. As all galaxies in A98 have the same distance modulus, the apparent magnitudes could reflect their intrinsic luminosities. For the bright and massive cluster galaxies in the core region of A98, their star formation activities have been reduced by some physical processes via environmental effects, such as galaxy-galaxy interaction, harassment, gas stripping, strangulation (Poggianti 2004; Yuan et al. 2005), which leads to a short SFR time scale. From Fig. 11b and Fig. 12b, no bright ($m_h < 16.5$) and central ($\Sigma > 0.4$ gal. arcmin^{-2}) galaxies are found to have the mean ISM metallicity less than 0.035, which is consistent with the ideas that more massive galaxies form fractionally more stars in a Hubble time than the low-mass counterparts, and metals are selectively lost from the faint galaxies with shallow potential wells via galactic winds (Tremonti et al. 2004).

We also try to find any trends of the star formation property along the distance from the main concentration of A98. However, no significant environmental effect is found, indicating that A98 is a dynamically complex cluster, and the clustercentric distance is not a good environmental indicator. An alterative explanation is that the star formation activities of the galaxies in a cluster with ongoing merger events might be more sensitive to the galaxy-scale gravitational interaction, not to the cluster-scale environment.

6 SUMMARY

A98 is a galaxy cluster with two large enhancements in X-ray surface brightness. This paper presents our optical photometric observation of A98 with the Beijing-Arizona-Taiwan-Connecticut (BATC) multicolor system. About 8,100 sources are detected down to $V \sim 20$ mag in a field of $58' \times 58'$ centered at this cluster, and their spectral energy distributions (SEDs) in 15 intermediate bands are obtained. There are 122 galaxies with spectroscopic redshifts in our field, among which 74 galaxies with $0.095 < z_{sp} < 0.115$ are selected as the members of A98. The dynamics of two substructures (A98N and A98S) is investigated with the help of the spectroscopic redshifts and the X-ray imaging data. A significant substructure, A98W, is found to the 10 arcmin west of A98S. Within our viewing field, a group of galaxies, A98X, which contains 21 galaxies with $z_{sp} \sim 0.120$, is located ~ 15 arcmin south of A98S. According to Newtonian gravitational binding criterion, A98X seems to be a separate system which is gravitationally unbound to A98.

After the star-galaxy separation by the color-color diagrams, a photometric redshift (z_{ph}) technique is applied to the galaxy sample for further membership determination. The color-magnitude relation is taken as a further restriction of the early-type cluster galaxies. As a result, 198 galaxies with $0.081 < z_{ph} < 0.113$ are selected as faint galaxy members of A98. Based on the enlarged member galaxies, the spatial distribution, localized velocity structure of A98 are discussed. The κ-test algorithm supports the existing substructures A98N and A98S, and the early suggested substructure, A98N, becomes more significant.

Assuming a Salpeter IMF and zero initial metallicity, the template SED library with different SFRs and redshifts has been built with the help of an evolutionary synthesis model, PEGASE. We fit the observed SED of 74 member galaxies with known spectroscopic redshifts one by one. The environmental effect on the star formation histories is found for these member galaxies. The bright massive galaxies in the core region of A98 are found to have shorter SFR time scales, longer mean stellar ages, and higher ISM metallicities, while the outlier galaxies are likely to have smaller stellar ages and longer SFR time scales. This effect is consistent with the existing correlations, such as the morphology-density relation, the luminosity-metallicity relation, and the mass-metallicity relation.

Acknowledgements We acknowledge the anonymous referee for his/her thorough reading of this paper and invaluable suggestions. This work was funded by the National Natural Science Foundation of China (NSFC) under Nos.10778618 and 10633020, and by the National Basic Research Program of China (973 Program) under No. 2007CB815403. This research has made use of the NED, which is operated

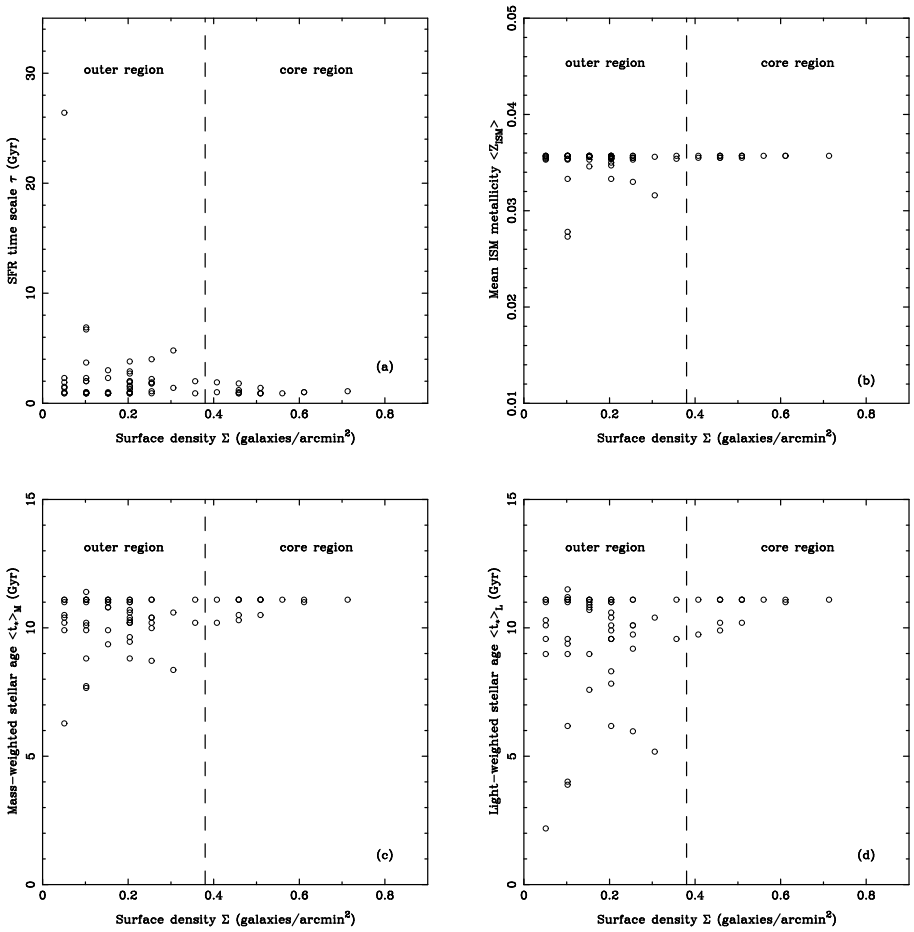

Fig. 11 Star formation properties for the galaxies with known z_{sp} in A98 as the functions of local surface density Σ. The star formation properties include the SFR time scale τ, metallicity, and the mean stellar ages weighted by mass and light.

by the Jet Propulsion Laboratory, California Institute of Technology, under contract with the National Aeronautics and Space Administration. We would like to thank Prof. Kong, X. at the University of Science and Technology of China for valuable discussion.

References

Abell, G. O. 1958, ApJS, 3, 211
Abell, G. O., Corwin, H. G., Jr., Olowin, R. P. 1989, ApJS, 70, 1
Allen, D. A. 1976, MNRAS, 174, 29
Beers, T. C., Geller, M. J., Huchra, J. P. 1982, ApJ, 257, 23 (BGH)
Beers, T. C., Gebhardt, K., Forman, W., Huchra, J. P., Jones, C. 1991, AJ, 102, 1581
Bettoni, D., Moles, M.,Kjærgaard, P., Fasano, G., & Varela, J. 2006, A&A, 452, 811
Bolzonella, M., Miralles, J.-M., & Pelló , R. 2000, A&A, 363, 476
Bower, R. G., Lucey, J. R., & Ellis, R. S. 1992, MNRAS, 254, 589
Brunner, R. J., Lubin, L. M. 2000, AJ, 120, 2851

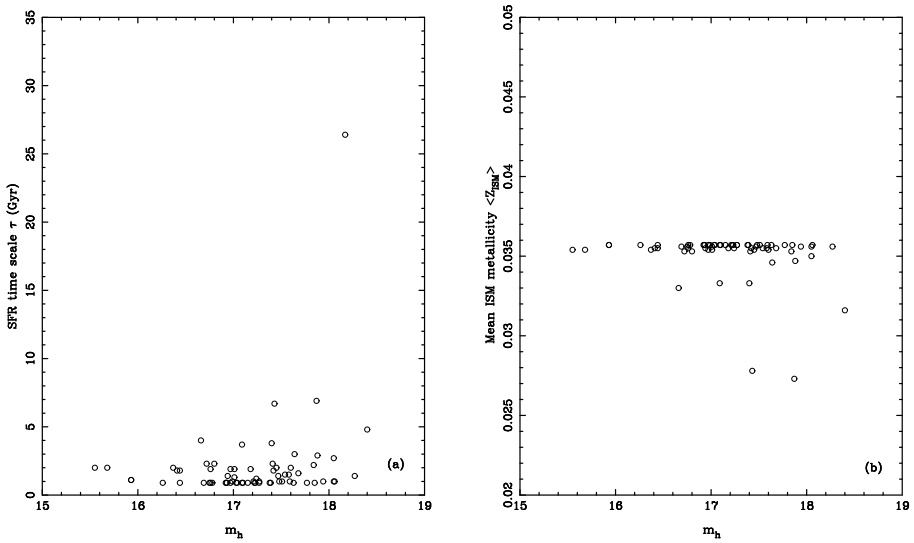

Fig. 12 The SFR time scales τ and mean ISM metallicities for the galaxies with known z_{sp} in A98 as the functions of magnitude in h band.

Bums, J.O., Rhee, G., Owen, F.N., & Pinkey, J. 1994, ApJ, 423, 94.
Colberg, J. M., White, S. D. M., et al. 2000, MNRAS, 319, 209
Colless, M., & Dunn, A. M. 1996, ApJ, 458, 435
Dressler, R. 1978a, ApJ, 223, 765
Dressler, R. 1978b, ApJ, 226, 55
Dressler, R. 1980, ApJ, 236, 351
Duus, A., & Newell, B. 1977, ApJS, 35, 209
Faber, S. M., Dressler, A. 1977, AJ, 82, 187
Fan, X., Burstein, D., Chen, J.-S., et al. 1996, AJ, 112, 628
Finoguenov, A., Guzzo, L., Hasinger, G., et al. 2007, ApJS, 172, 182
Fioc, M., & Rocca-Volmerange, B. 1997, A&A, 326, 950
Fioc, M., & Rocca-Volmerange, B. 1999, A&A, 351, 869
Forman, W., Bechtold, J., Blair, W., Giacconi, R., van Speybroeck, L., Jones, C. 1981, ApJ, 243, L133
Forman, W.,& Jones, C. 1982, ARA&A, 20, 547
Garnett, D. R., & Shields, G. A. 1987, ApJ, 317, 82
Geller, M. J., & Peebles, P. J. E. 1973, ApJ, 184, 329
Goto, T., Postman, M., Cross, N.J.G., et al. 2005, ApJ, 621, 188
Gunn, J. E., & Stryker, L. L. 1983, ApJS, 52, 121
Henry, J.P. & Briel, U.G. 1993, Adv. Space Res. 13, (12)191.
Henry, J. P., Henriksen, M. J., Charles, P. A., Thorstensen, M. J. 1981, ApJ, 243, L137
Ilbert, O., Capak, P., Salvato, M., et al. 2009, ApJ, 690,1236
Jones, C., & Forman, W. 1999, ApJ, 511, 65
Kauffmann, G., Colberg, J. M., Diaferio, A., White, S. D. M. 1999, MNRAS, 307, 529
Krempeć-Krygier, J.,& Krygier, B. 1995, A&A, 296, 359 (KK95)
Lequeux, J., Rayo, J. F., Serrano, A., Peimbert, M., & Torres-Peimbert, S. 1979, A&A, 80, 155
Melbourne, J., & Salzer, J. J. 2002, AJ, 123, 2302
Oegerle, W. R., & Hill, J. M. 1994, AJ, 107, 857
Pelló, R., Kneib, J. P., Le Borgne, et al. 1999a, A&A, 346, 359
Pelló, R., Kneib, J. P., Bolzonella, M., Miralles, J. M. 1999b, ASP Conf. Ser., 191, 241

Pinkney, J., Burns, J. O., Ledlow, M. J., et al. 2000, AJ, 120, 2269 (PBLGH)
Poggianti, B. 2004, Proceedings of ”Baryons in Dark Matter Halos”. Novigrad, Croatia, 5-9 Oct 2004. Editors: R. Dettmar, U. Klein, P. Salucci. Published by SISSA, Proceedings of Science, p.104.1
Rhee, G. F. R. N., van Haarlem, M.P., Katgert, P. 1991, A&A, 233,325
Rowan-Robinson, M., et al. 2008, MNRAS, 386, 697
Salpeter, E. E. 1955, ApJ, 121, 161
Salvador-Solé, E., Gonzáles-Casado, G., Solanes, J.M. 1993, ApJ, 410, 1
Sarazin, C. L. 1992, in: Cluster and Superclusters of Galaxies, ed. A.C.Fabian, Dordrecht: Kluwer, p. 131
Schechter, P. 1976, ApJ, 203, 297
Struble, M. F., & Rood, H. J. 1999, ApJS, 125, 35
Tremonti, C. A., et al. 2004, ApJ, 613, 898
West, M. J., Villumsen, J. V., Dekel, A. 1991, ApJ, 369, 287
West, M. J., Jones, C., Forman, W. 1995, ApJ, 451, L5
Xia, L. -F., Zhou, X., Ma, J., et al. 2002, PASP, 114, 1349
Yang, Y.-B., Zhou, X., Yuan, Q.-R., Jiang, Z.-J., Ma, J., Wu, H., Chen, J.-S. 2004, ApJ, 600, 141
Yuan, Q.-R., Zhou, X., Chen, J.-S., Jiang, Z.-J., Ma, J., Wu, H., Xue, S.-J., Zhu, J. 2001, AJ, 122, 1718
Yuan, Q.-R., Zhou, X., Jiang, Z.-J. 2003, ApJS, 149, 53
Yuan, Q.-R., Zhao, L.-F., Yang, Y.B., et al. 2005, AJ, 130, 2559
Zabludoff, A. I., Huchra, J. P., Geller, M. J. 1990, ApJS, 74, 1
Zeldovich, I. B., Einasto, J., Shandarin, S. F. 1982, Nature, 300, 407
Zhou, X., Chen, J.-S., Xu, W., et al.1999, PASP, 111, 909
Zhou, X., Jiang, Z.-J., Xue, S.-J., Wu, H., Ma, J., Chen, J.-S. 2001, ChJAA (Chin. J. Astron. Astrophys.), 1, 372
Zhou, X., Jiang, Z.-J., Ma, J., Xue, S.-J., Wu, H., Chen, J.-S., Zhu, J., Sun, W.-S., Windhorst, R. A. 2003a, A&A, 397, 361
Zhou, X., Arimoto, N., Tanaka, I., Jiang, Z.-J., Chen, J.-S. 2003b, PASJ, 55, 891

Table 3. Catalog of 198 newly-selected candidates of member galalxies in A98

No.	R.A.	Decl.	z_{ph}	T	a	b	c	d	e	f	g	h	i	j	k	m	n	o	p
1	0 45 07.54	20 30 39.10	0.102	2	20.94	20.72	20.26	19.67	19.26	18.93	18.69	18.42	18.20	18.22	18.01	17.85	17.71	17.52	17.43
2	0 45 08.17	20 28 21.70	0.099	5	19.52	19.01	18.86	18.32	18.17	18.04	17.95	17.82	17.65	17.66	17.61	17.48	17.35	17.26	17.03
3	0 45 11.31	20 27 23.60	0.094	3	20.09	20.42	20.03	18.91	18.87	18.68	18.45	18.30	18.14	18.12	17.87	17.89	17.67	17.66	17.76
4	0 45 22.06	20 29 56.40	0.087	1	19.93	19.34	19.20	18.70	18.40	18.34	18.19	18.16	18.01	17.72	17.82	17.81	17.77	17.62	17.52
5	0 45 24.39	20 39 56.80	0.082	3	20.21	19.71	19.66	19.28	19.05	19.03	18.83	18.78	18.66	18.57	18.55	18.54	18.48	18.93	18.60
6	0 45 24.63	20 26 22.90	0.099	2	20.15	19.47	19.38	18.46	17.92	17.65	17.41	17.24	17.01	16.98	16.83	16.73	16.60	16.42	16.30
7	0 45 24.77	20 41 06.10	0.092	2	20.51	19.27	19.22	18.55	18.21	17.92	17.65	17.45	17.19	17.15	16.96	16.85	16.71	16.58	16.51
8	0 45 25.61	20 30 51.10	0.101	1	20.23	18.91	18.94	17.94	17.46	17.22	17.02	16.81	16.61	16.32	16.45	16.34	16.17	16.07	15.99
9	0 45 31.61	20 22 56.20	0.089	1	19.37	18.71	18.50	18.08	18.00	17.86	17.71	17.64	17.62	17.58	17.64	17.56	17.51	17.50	17.39
10	0 45 33.45	20 42 21.90	0.092	1	20.87	19.76	19.31	18.61	18.18	17.90	17.71	17.51	17.30	17.19	17.16	17.01	16.90	16.82	16.72
11	0 45 33.87	20 24 54.90	0.109	4	20.71	20.45	20.25	19.55	19.60	19.40	19.30	19.19	18.94	19.28	18.89	18.97	18.86	18.69	18.39
12	0 45 34.15	20 42 13.30	0.100	1	21.61	21.22	20.71	20.34	19.86	19.44	19.25	19.04	18.97	18.62	18.74	18.72	18.58	18.49	18.37
13	0 45 38.09	20 39 56.00	0.086	1	22.06	21.12	20.59	20.05	19.29	18.89	18.55	18.43	18.15	18.07	17.90	17.80	17.73	17.58	17.36
14	0 45 39.48	20 18 25.70	0.089	1	21.20	21.80	20.96	20.19	19.55	19.35	19.12	18.91	18.57	18.49	18.55	18.29	18.37	18.18	17.91
15	0 45 41.68	20 34 10.30	0.090	3	19.86	19.95	19.79	18.89	18.57	18.42	18.20	18.00	17.83	17.98	17.58	17.57	17.40	17.33	17.40
16	0 45 45.13	20 36 18.40	0.094	7	20.20	20.26	20.26	19.30	19.66	19.42	19.53	19.21	19.12	19.40	19.20	18.82	18.88	19.33	18.75
17	0 45 45.64	20 43 24.70	0.106	1	20.63	20.52	20.49	19.62	19.20	18.82	18.55	18.35	18.14	18.03	17.95	17.96	17.81	17.67	17.63
18	0 45 45.90	20 18 45.80	0.093	4	20.09	19.77	19.58	18.89	18.84	18.67	18.44	18.36	18.14	18.17	18.06	17.90	17.79	17.69	17.69
19	0 45 46.09	20 23 30.80	0.093	1	20.91	19.86	19.90	18.86	18.58	18.32	18.14	17.99	17.74	17.72	17.57	17.45	17.40	17.21	17.27
20	0 45 46.13	20 28 48.10	0.097	2	20.45	20.69	20.12	19.04	18.56	18.24	18.06	17.88	17.65	17.66	17.53	17.37	17.21	17.11	16.97
21	0 45 47.17	20 29 51.20	0.086	1	20.40	19.74	19.20	18.34	18.17	18.07	17.77	17.68	17.61	17.45	17.59	17.46	17.43	17.42	17.21
22	0 45 47.30	20 26 54.30	0.084	1	18.67	17.86	17.54	16.85	16.56	16.44	16.18	16.09	15.91	15.92	15.80	15.73	15.63	15.51	15.57
23	0 45 47.44	20 34 03.80	0.112	1	21.73	20.48	20.86	19.85	19.58	19.33	19.12	18.95	18.79	18.82	18.58	18.59	18.46	18.13	18.38
24	0 45 47.95	20 36 47.30	0.101	4	21.62	20.99	24.61	20.81	20.81	20.75	20.52	20.16	20.36	20.01	20.12	20.18	20.09	19.67	18.92
25	0 45 48.35	20 43 24.30	0.096	3	21.32	20.16	20.86	19.67	19.34	19.39	19.27	18.95	18.68	18.63	18.52	18.45	18.38	18.15	18.17
26	0 45 50.74	20 18 07.90	0.084	3	20.50	19.80	19.62	18.65	18.22	18.07	17.85	17.67	17.48	17.41	17.28	17.15	17.12	16.87	16.79
27	0 45 53.08	20 12 59.70	0.089	3	20.99	20.49	20.42	19.64	19.34	19.12	18.94	18.74	18.56	18.47	18.26	18.26	18.01	18.13	17.94
28	0 45 55.14	20 26 57.50	0.085	2	20.90	19.85	19.72	18.78	18.28	17.98	17.78	17.56	17.38	17.15	17.10	16.98	16.84	16.78	16.64
29	0 45 55.17	20 29 59.50	0.086	4	19.90	20.34	19.61	18.98	18.86	18.74	18.49	18.39	18.18	18.11	17.95	17.94	17.83	17.75	17.71
30	0 45 55.67	20 28 38.10	0.095	2	20.67	19.61	19.62	18.76	18.31	18.07	17.82	17.63	17.42	17.35	17.22	17.12	16.98	16.79	16.85
31	0 45 56.39	20 43 21.50	0.095	1	20.53	19.25	19.20	18.35	17.89	17.57	17.36	17.23	17.02	16.94	16.88	16.73	16.64	16.50	16.36
32	0 45 57.54	20 37 00.80	0.098	3	19.90	19.16	18.99	18.44	18.09	17.86	17.70	17.52	17.29	17.24	17.10	16.99	16.87	16.72	16.61
33	0 45 57.59	20 36 55.30	0.096	3	19.41	18.77	18.63	17.95	17.64	17.45	17.26	17.08	16.85	16.84	16.67	16.56	16.44	16.28	16.20
34	0 45 58.53	20 29 17.50	0.090	3	21.64	20.39	20.84	19.33	19.09	19.06	18.81	18.61	18.35	18.17	18.15	18.04	17.89	17.76	17.68
35	0 45 58.54	20 21 37.40	0.097	1	20.54	20.22	20.09	19.02	18.89	18.65	18.49	18.38	18.18	18.14	18.01	17.99	17.92	17.75	17.69
36	0 45 59.60	20 17 58.80	0.090	3	20.13	20.19	19.86	18.97	18.71	18.53	18.28	18.17	17.99	17.85	17.79	17.72	17.51	17.53	17.25
37	0 46 00.13	20 20 32.20	0.101	2	21.13	20.53	20.07	19.32	18.73	18.45	18.24	18.07	17.82	17.86	17.67	17.57	17.45	17.24	17.16
38	0 46 01.41	20 30 13.30	0.106	3	20.62	21.42	20.31	19.13	18.98	18.70	18.60	18.40	18.14	18.17	17.97	17.89	17.83	17.57	17.58
39	0 46 01.76	20 21 27.50	0.089	1	18.82	18.17	18.02	17.60	17.54	17.40	17.28	17.26	17.23	17.16	17.17	17.19	17.17	17.24	17.04
40	0 46 01.81	20 36 38.00	0.104	5	20.86	20.23	20.53	19.86	19.72	19.61	19.61	19.43	19.21	19.24	19.34	19.16	19.25	19.10	18.64
41	0 46 02.73	20 36 06.20	0.098	7	19.57	19.19	19.22	18.58	18.45	18.45	18.38	18.31	18.19	18.24	18.08	18.05	17.90	17.97	17.96

Table 3—Continued

No.	R.A.	Decl.	z_{ph}	T	a	b	c	d	e	f	g	h	i	j	k	m	n	o	p
42	0 46 03.37	20 28 08.40	0.108	1	21.45	20.46	19.87	19.47	19.06	18.78	18.51	18.36	18.14	18.11	18.02	17.90	17.73	17.63	17.63
43	0 46 04.88	20 43 58.50	0.100	3	21.40	20.97	20.79	20.17	20.04	19.64	19.49	19.36	19.16	19.10	18.94	18.78	18.74	18.46	18.24
44	0 46 06.64	20 25 57.20	0.087	1	19.73	19.14	18.76	18.12	17.96	17.90	17.73	17.62	17.53	17.56	17.45	17.35	17.40	17.28	17.28
45	0 46 07.55	20 28 46.40	0.099	1	20.35	19.34	19.35	18.24	17.79	17.44	17.23	17.03	16.81	16.75	16.68	16.56	16.42	16.25	16.22
46	0 46 07.73	20 28 27.00	0.101	2	20.53	20.53	20.97	19.80	19.08	18.82	18.69	18.49	18.26	18.17	18.14	18.03	17.84	17.75	17.67
47	0 46 10.80	20 40 41.00	0.100	3	18.98	18.74	18.35	17.46	17.65	16.88	16.86	16.67	16.72	15.78	16.31	16.18	16.14	16.00	15.72
48	0 46 10.92	20 37 11.90	0.096	7	19.84	19.59	19.40	18.85	19.04	18.94	18.90	18.84	18.70	18.59	18.72	18.57	18.40	18.58	18.69
49	0 46 11.16	20 22 11.60	0.106	1	20.02	19.41	19.34	18.75	18.72	18.58	18.59	18.57	18.47	18.35	18.44	18.38	18.57	18.33	17.95
50	0 46 12.59	20 26 57.40	0.105	1	19.14	18.68	18.62	18.10	18.02	17.89	17.72	17.66	17.54	17.54	17.49	17.47	17.48	17.39	17.49
51	0 46 12.71	20 30 41.70	0.095	2	20.40	19.77	19.57	18.86	18.43	18.14	17.90	17.70	17.47	17.40	17.26	17.13	17.01	16.83	16.76
52	0 46 13.48	20 19 25.60	0.094	1	18.74	18.71	18.23	16.84	17.13	16.43	16.41	16.25	16.18	14.60	16.04	15.76	15.67	16.08	15.33
53	0 46 13.55	20 36 11.90	0.085	7	19.24	19.04	18.81	18.50	18.36	18.30	18.24	18.21	18.10	18.01	18.01	17.88	17.85	17.81	17.99
54	0 46 15.10	20 29 56.70	0.089	1	21.24	20.28	20.21	19.29	18.69	18.43	18.10	17.96	17.74	17.64	17.54	17.45	17.23	17.16	17.07
55	0 46 15.40	20 44 16.30	0.101	1	22.48	21.88	22.92	20.54	20.09	19.93	19.86	19.71	19.58	19.11	19.41	19.46	19.40	19.05	18.72
56	0 46 15.70	20 32 07.40	0.087	1	20.19	19.85	19.61	18.82	18.49	18.24	17.95	17.83	17.61	17.71	17.49	17.35	17.24	17.11	17.05
57	0 46 15.97	20 30 55.50	0.096	1	20.78	19.89	19.91	19.04	19.12	18.97	18.82	18.75	18.75	18.39	18.75	18.54	18.61	18.41	18.21
58	0 46 16.25	20 32 35.10	0.086	2	21.40	20.68	20.67	19.76	19.40	18.94	18.66	18.51	18.33	18.23	18.03	17.96	17.94	17.74	17.54
59	0 46 16.77	20 32 01.30	0.101	1	20.68	21.17	21.78	19.88	19.89	19.28	18.96	18.74	18.59	18.79	18.32	18.35	18.31	18.05	17.92
60	0 46 17.91	20 37 35.50	0.104	3	22.52	20.98	20.96	20.36	20.58	19.80	19.67	19.38	19.27	19.41	19.37	18.94	18.83	18.66	18.28
61	0 46 17.97	20 32 34.60	0.096	1	19.65	19.24	19.07	18.40	18.23	18.11	17.99	17.88	17.78	17.50	17.65	17.55	17.51	17.38	17.37
62	0 46 18.20	20 42 15.90	0.092	3	20.18	19.44	19.23	18.58	18.17	17.95	17.77	17.61	17.42	17.34	17.21	17.13	16.98	16.88	16.82
63	0 46 18.77	20 24 49.10	0.109	1	22.85	22.05	21.84	20.36	20.78	20.46	20.31	19.94	19.77	19.57	19.74	19.80	19.35	19.74	19.27
64	0 46 20.84	20 21 27.30	0.085	7	21.44	20.87	20.93	20.13	20.10	19.92	19.97	19.83	19.72	19.36	19.26	19.33	19.56	19.72	18.87
65	0 46 20.91	20 31 01.10	0.088	1	21.20	21.38	20.99	19.98	19.34	19.11	18.93	18.74	18.56	18.63	18.48	18.26	18.21	18.06	18.05
66	0 46 21.31	20 43 33.80	0.087	1	20.87	20.11	19.89	18.97	18.52	18.32	18.14	17.98	17.72	17.74	17.52	17.42	17.45	17.23	17.21
67	0 46 22.36	20 25 15.50	0.110	2	20.66	19.89	19.90	18.82	18.54	18.21	18.03	17.84	17.57	17.60	17.38	17.32	17.22	16.97	17.03
68	0 46 22.56	20 23 30.00	0.082	1	20.54	20.16	19.76	19.40	19.31	19.32	19.14	19.16	19.01	19.14	18.87	18.98	18.96	19.18	18.86
69	0 46 22.63	20 34 11.40	0.101	1	22.00	20.29	20.81	20.11	19.34	19.08	18.82	18.61	18.49	18.41	18.22	18.22	17.90	17.88	17.73
70	0 46 23.28	20 29 38.90	0.090	1	21.98	20.67	20.45	19.42	18.79	18.47	18.31	18.05	17.81	17.75	17.59	17.44	17.37	17.26	17.18
71	0 46 23.64	20 37 28.40	0.097	1	21.78	20.55	20.43	19.25	18.72	18.18	18.03	17.89	17.62	17.34	17.45	17.31	17.29	17.08	17.04
72	0 46 24.35	20 37 36.30	0.087	1	20.63	20.28	20.12	18.78	18.33	18.05	17.81	17.66	17.49	17.05	17.30	17.20	17.16	17.05	16.98
73	0 46 24.55	20 30 02.50	0.096	1	20.45	19.84	19.62	18.57	18.22	17.93	17.69	17.50	17.27	17.04	17.09	17.00	16.83	16.76	16.69
74	0 46 24.76	20 36 59.00	0.085	2	20.86	20.39	20.75	19.65	19.08	18.79	18.56	18.47	18.33	17.79	18.05	17.95	17.85	17.73	17.45
75	0 46 25.03	20 22 48.50	0.106	4	21.26	21.77	20.89	20.41	20.62	19.88	19.87	19.66	19.54	19.53	19.24	19.36	19.49	18.83	18.40
76	0 46 25.13	20 29 06.60	0.097	2	21.41	20.17	20.25	19.12	18.78	18.40	18.13	17.98	17.75	17.67	17.45	17.39	17.24	17.06	16.97
77	0 46 25.63	20 30 33.80	0.105	2	20.14	19.82	19.96	18.96	18.54	18.19	18.02	17.82	17.57	17.55	17.38	17.30	17.16	16.99	16.91
78	0 46 26.68	20 28 17.40	0.106	1	21.63	20.76	21.20	19.52	19.08	18.66	18.39	18.29	17.99	18.05	17.83	17.80	17.55	17.41	17.36
79	0 46 26.76	20 21 44.70	0.086	1	19.15	18.51	18.38	17.82	17.59	17.58	17.40	17.32	17.24	17.14	17.18	17.11	17.11	17.02	17.03
80	0 46 27.41	20 35 40.00	0.090	3	20.15	20.25	20.75	19.44	19.20	19.00	18.84	18.67	18.43	18.30	18.13	18.09	18.01	17.92	17.66
81	0 46 27.88	20 30 51.60	0.094	1	20.88	19.81	20.66	19.06	18.69	18.38	18.19	18.01	17.72	17.68	17.52	17.43	17.36	17.20	17.10
82	0 46 28.05	20 17 16.70	0.093	7	21.07	20.55	20.22	19.75	19.74	19.55	19.60	19.40	19.35	19.18	19.06	19.14	19.12	19.13	18.45

Table 3—Continued

No.	R.A.	Decl.	z_{ph}	T	a	b	c	d	e	f	g	h	i	j	k	m	n	o	p
83	0 46 28.06	20 17 29.00	0.090	4	19.83	19.40	19.28	18.57	18.39	18.27	18.12	18.02	17.79	17.80	17.60	17.56	17.45	17.42	17.43
84	0 46 28.30	20 27 59.80	0.086	1	19.11	18.49	18.18	17.52	17.28	17.12	16.91	16.80	16.65	16.50	16.55	16.47	16.45	16.37	16.33
85	0 46 28.37	20 28 10.70	0.098	1	20.76	20.47	20.32	19.06	18.68	18.30	18.14	17.96	17.74	17.26	17.64	17.46	17.33	17.23	17.09
86	0 46 28.93	20 27 53.80	0.101	1	20.92	19.91	19.76	18.62	18.30	17.88	17.64	17.44	17.22	16.76	17.05	16.93	16.77	16.64	16.52
87	0 46 29.03	20 26 11.80	0.105	1	19.75	19.42	19.59	18.71	18.61	18.51	18.35	18.24	18.18	17.97	18.15	18.10	17.98	17.94	17.82
88	0 46 29.05	20 26 02.90	0.110	1	21.14	21.75	20.45	19.44	19.30	19.05	18.87	18.70	18.46	18.37	18.37	18.35	18.10	17.93	17.73
89	0 46 29.14	20 30 08.00	0.099	1	20.54	19.80	19.48	18.79	18.47	18.18	18.02	17.77	17.57	17.59	17.39	17.32	17.20	17.09	17.07
90	0 46 29.23	20 29 20.80	0.100	3	18.69	18.36	17.83	16.98	17.21	16.62	16.51	16.39	16.26	14.93	15.91	15.63	15.56	15.47	15.25
91	0 46 29.34	20 27 30.20	0.108	3	20.40	20.12	19.48	19.07	18.79	18.46	18.33	18.16	17.87	17.98	17.68	17.64	17.57	17.37	17.30
92	0 46 29.43	20 26 09.50	0.106	1	20.33	20.05	19.66	18.84	18.74	18.54	18.34	18.26	18.14	17.95	18.07	18.00	17.74	17.72	17.62
93	0 46 29.53	20 42 50.60	0.098	2	20.40	20.60	19.93	19.22	18.78	18.49	18.34	18.13	17.90	17.66	17.86	17.65	17.56	17.42	17.27
94	0 46 29.74	20 39 00.30	0.096	2	19.73	18.75	18.60	17.71	17.15	16.85	16.66	16.45	16.21	16.17	16.03	15.93	15.75	15.62	15.54
95	0 46 29.82	20 19 00.40	0.096	6	21.68	20.95	21.46	20.18	20.44	20.34	20.06	20.19	19.99	20.23	19.90	19.87	19.53	19.87	19.02
96	0 46 29.84	20 42 38.80	0.093	1	20.46	19.25	19.03	18.50	18.21	18.08	17.99	17.75	17.61	17.16	17.50	17.33	17.30	17.18	17.14
97	0 46 30.00	20 38 52.10	0.110	1	20.33	19.26	19.25	18.07	17.59	17.26	17.09	16.87	16.65	16.56	16.45	16.38	16.18	16.05	16.06
98	0 46 30.00	20 37 04.40	0.088	1	20.42	19.43	19.19	18.57	18.13	17.81	17.58	17.43	17.22	17.11	17.03	16.90	16.80	16.69	16.62
99	0 46 30.22	20 36 41.20	0.094	1	20.91	20.08	19.88	18.62	18.18	17.86	17.70	17.48	17.26	16.96	17.12	16.99	16.95	16.75	16.58
100	0 46 30.34	20 16 36.40	0.091	1	22.92	21.70	21.19	19.78	19.68	19.35	19.23	19.07	18.92	18.64	18.80	18.65	18.43	18.48	18.23
101	0 46 30.36	20 17 00.30	0.096	3	20.57	20.06	19.98	19.09	18.80	18.62	18.51	18.33	18.13	18.15	17.92	17.90	17.74	17.67	17.50
102	0 46 30.44	20 14 41.50	0.097	1	22.20	20.61	21.22	19.64	18.99	18.55	18.37	18.12	17.87	17.95	17.70	17.52	17.39	17.25	17.23
103	0 46 30.51	20 39 01.00	0.094	1	21.33	20.49	21.09	19.30	19.03	18.67	18.48	18.25	18.06	17.49	17.83	17.75	17.53	17.56	17.48
104	0 46 30.64	20 38 57.70	0.094	1	21.53	20.26	21.64	19.64	19.27	18.98	18.77	18.47	18.31	17.72	18.04	18.01	17.83	17.79	17.77
105	0 46 31.58	20 35 21.70	0.094	1	20.25	19.87	19.84	18.80	18.62	18.51	18.37	18.29	18.14	18.01	18.05	17.85	17.91	17.63	17.82
106	0 46 31.84	20 37 40.00	0.091	2	20.95	19.91	19.78	18.96	18.20	17.96	17.78	17.56	17.36	17.27	17.14	17.04	16.92	16.77	16.56
107	0 46 32.19	20 28 05.80	0.101	1	21.28	20.18	20.18	18.95	18.47	18.19	17.99	17.78	17.50	17.38	17.43	17.29	17.15	16.99	17.02
108	0 46 32.79	20 26 58.70	0.094	1	20.90	20.62	20.74	19.36	19.29	18.76	18.53	18.32	18.14	17.99	17.90	17.80	17.64	17.58	17.52
109	0 46 33.38	20 23 58.30	0.094	2	21.48	20.07	20.21	19.13	18.74	18.43	18.23	17.93	17.77	17.42	17.48	17.38	17.24	17.13	16.94
110	0 46 34.04	20 34 41.60	0.087	7	21.21	21.08	19.92	20.30	20.42	20.08	20.11	20.43	19.40	20.04	19.94	20.76	20.36	21.50	18.84
111	0 46 34.08	20 23 04.20	0.094	1	21.34	21.08	20.85	19.58	19.29	19.00	18.77	18.59	18.43	18.33	18.25	18.15	17.94	17.88	17.85
112	0 46 34.28	20 47 57.70	0.107	2	21.44	20.19	19.49	19.42	18.79	18.45	18.24	18.03	17.79	17.66	17.60	17.48	17.26	17.12	16.97
113	0 46 34.30	20 28 07.40	0.094	1	20.12	19.58	19.81	18.76	18.15	17.88	17.64	17.46	17.16	17.21	17.03	16.88	16.77	16.62	16.56
114	0 46 34.44	20 30 10.80	0.092	1	22.11	20.18	21.00	19.49	19.13	18.80	18.55	18.39	18.21	18.17	18.06	17.92	17.69	17.67	17.57
115	0 46 34.63	20 28 08.40	0.094	1	20.78	19.24	19.68	18.75	18.01	17.78	17.52	17.37	17.05	17.13	16.94	16.80	16.67	16.52	16.39
116	0 46 35.75	20 34 36.60	0.100	1	21.62	20.24	20.05	19.48	19.03	18.50	18.39	18.18	17.99	18.03	17.82	17.66	17.54	17.43	17.37
117	0 46 35.79	20 28 32.30	0.100	2	20.87	20.05	19.45	18.61	18.21	17.79	17.58	17.41	17.20	16.88	16.93	16.83	16.62	16.51	16.40
118	0 46 36.10	20 38 40.20	0.093	2	20.36	19.55	19.34	18.74	18.25	18.06	17.89	17.67	17.50	17.38	17.26	17.22	17.10	16.96	16.89
119	0 46 36.16	20 28 05.60	0.094	1	21.46	20.02	19.74	18.91	18.40	18.14	17.85	17.70	17.48	17.40	17.38	17.24	17.13	16.96	16.98
120	0 46 36.33	20 33 54.90	0.090	1	19.80	19.36	19.15	18.27	18.23	18.06	17.85	17.76	17.64	17.64	17.50	17.48	17.42	17.36	17.30
121	0 46 36.67	20 32 31.60	0.089	3	21.02	20.31	20.86	19.69	19.44	19.18	19.02	18.88	18.69	18.73	18.55	18.34	18.29	18.18	17.98
122	0 46 36.89	20 46 23.30	0.103	3	20.73	19.75	19.27	18.74	18.25	17.98	17.76	17.61	17.39	17.30	17.21	17.10	16.98	16.76	16.76
123	0 46 37.00	20 20 45.20	0.100	4	22.37	21.30	19.75	20.01	19.77	19.51	19.52	19.32	19.00	19.10	18.75	18.87	18.65	18.72	18.35

Table 3—Continued

No.	R.A.	Decl.	z_{ph}	T	a	b	c	d	e	f	g	h	i	j	k	m	n	o	p
124	0 46 37.03	20 40 04.10	0.106	3	21.47	20.48	20.89	19.94	19.80	19.50	19.39	19.10	18.89	18.79	18.54	18.65	18.62	18.17	18.02
125	0 46 37.06	20 36 31.30	0.095	3	20.09	19.65	19.42	18.62	18.38	18.19	18.04	17.88	17.69	17.46	17.50	17.36	17.24	17.11	17.16
126	0 46 37.07	20 36 36.50	0.094	3	20.09	19.27	19.06	18.41	18.11	17.90	17.78	17.61	17.39	17.27	17.17	17.06	16.97	16.81	16.77
127	0 46 37.09	20 36 41.10	0.092	3	20.70	19.35	19.46	18.79	18.41	18.24	18.09	17.94	17.69	17.61	17.42	17.35	17.25	17.12	16.99
128	0 46 37.27	20 35 37.50	0.095	3	21.00	21.64	20.43	20.23	20.23	19.60	19.54	19.35	19.17	18.97	19.17	18.85	18.67	18.85	17.88
129	0 46 37.43	20 18 18.90	0.094	1	18.34	18.42	17.80	17.09	17.56	16.84	17.19	16.80	17.13	15.10	16.87	16.60	16.43	16.90	16.28
130	0 46 37.85	20 35 35.50	0.087	3	20.59	20.30	19.89	19.13	18.94	18.56	18.37	18.22	18.07	18.18	17.89	17.73	17.65	17.55	17.31
131	0 46 38.21	20 22 54.50	0.098	1	20.04	19.17	19.02	18.16	17.75	17.53	17.29	17.13	16.90	16.82	16.73	16.66	16.49	16.38	16.36
132	0 46 38.40	20 29 38.70	0.100	1	22.39	20.84	21.84	20.25	20.17	19.65	19.63	19.22	19.01	19.40	18.97	18.80	18.78	18.64	18.35
133	0 46 38.52	20 18 28.30	0.094	1	17.78	17.61	17.23	16.41	16.75	16.28	16.14	16.09	16.04	14.66	16.07	15.81	15.78	16.14	15.50
134	0 46 38.62	20 22 45.50	0.100	1	20.58	19.55	19.52	18.54	18.17	17.79	17.63	17.44	17.22	16.96	17.06	16.96	16.81	16.71	16.64
135	0 46 42.40	20 27 55.30	0.110	1	20.38	21.00	20.28	19.25	19.47	19.16	19.00	18.93	18.74	18.92	18.69	18.65	18.61	18.41	18.36
136	0 46 42.50	20 35 11.40	0.087	1	22.61	21.74	21.41	20.17	20.04	19.88	19.86	19.64	19.30	19.42	19.24	19.09	18.90	19.42	18.72
137	0 46 42.67	20 15 18.20	0.111	1	20.94	20.16	19.89	19.33	18.87	18.44	18.29	18.17	17.91	17.86	17.77	17.68	17.59	17.38	17.25
138	0 46 42.79	20 45 04.60	0.098	2	20.90	20.68	20.60	19.34	19.00	18.65	18.46	18.25	18.00	17.94	17.85	17.71	17.61	17.42	17.28
139	0 46 43.09	20 13 46.20	0.110	1	21.85	20.34	20.48	19.46	18.91	18.63	18.59	18.31	18.04	17.96	17.93	17.87	17.69	17.54	17.44
140	0 46 43.12	20 29 45.00	0.091	3	20.98	20.03	19.46	18.84	18.48	18.22	18.01	17.89	17.64	17.51	17.43	17.32	17.22	17.07	17.02
141	0 46 43.65	20 36 20.70	0.096	2	20.20	19.72	19.73	18.82	18.58	18.47	18.34	18.11	17.97	17.97	17.86	17.81	17.77	17.61	17.51
142	0 46 44.27	20 27 03.50	0.108	3	20.55	20.39	20.12	19.42	19.06	18.84	18.65	18.53	18.22	18.26	18.04	17.98	17.83	17.65	17.54
143	0 46 44.28	20 18 00.50	0.084	1	18.92	18.25	17.74	16.93	16.75	16.64	16.30	16.22	16.06	16.00	15.94	15.84	15.81	15.74	15.71
144	0 46 44.43	20 18 12.40	0.086	2	21.67	21.81	20.48	20.09	19.53	19.20	19.03	18.80	18.62	17.91	18.50	18.24	18.21	18.14	17.90
145	0 46 45.62	20 35 19.80	0.096	1	22.06	21.13	20.48	19.88	19.51	19.35	19.10	19.01	18.77	18.76	18.61	18.63	18.47	18.39	18.16
146	0 46 45.88	20 37 25.70	0.094	3	20.19	20.43	20.93	19.37	19.42	18.90	18.80	18.63	18.41	18.09	18.10	17.94	17.78	17.81	17.58
147	0 46 46.55	20 28 32.00	0.101	6	19.73	19.36	19.29	18.77	18.65	18.53	18.41	18.29	18.13	18.21	17.97	17.93	17.90	17.69	17.74
148	0 46 47.53	20 28 52.00	0.095	7	20.04	20.11	19.59	19.16	19.53	19.17	19.17	19.10	18.99	19.18	18.78	18.82	19.21	18.79	18.92
149	0 46 47.61	20 30 47.60	0.094	2	21.49	20.44	20.61	19.09	18.77	18.42	18.21	18.06	17.82	17.63	17.61	17.54	17.38	17.30	16.96
150	0 46 48.01	20 22 44.90	0.091	2	21.48	20.31	20.54	19.48	19.16	18.81	18.60	18.60	18.38	18.27	18.06	18.03	17.94	17.73	17.72
151	0 46 48.52	20 15 06.50	0.094	1	19.95	19.38	19.14	18.40	18.20	18.07	17.93	17.82	17.67	17.70	17.55	17.50	17.37	17.31	17.32
152	0 46 48.57	20 29 45.50	0.087	1	20.15	19.36	19.25	18.81	18.62	18.60	18.47	18.44	18.29	18.43	18.33	18.29	18.35	18.23	18.03
153	0 46 48.69	20 31 24.70	0.100	2	20.39	19.89	19.87	18.88	18.43	18.17	17.99	17.77	17.53	17.43	17.30	17.21	17.01	16.87	16.88
154	0 46 48.82	20 15 08.00	0.090	1	20.02	19.56	19.14	18.45	18.29	18.15	17.95	17.90	17.74	17.69	17.61	17.55	17.41	17.38	17.41
155	0 46 49.03	20 25 37.60	0.082	1	21.33	21.23	20.40	19.64	19.26	19.18	18.94	18.93	18.64	18.73	18.43	18.37	18.32	18.15	18.20
156	0 46 49.30	20 28 10.70	0.100	2	20.51	20.86	20.51	19.58	19.57	19.00	18.75	18.60	18.37	18.41	18.18	18.07	18.04	17.80	17.62
157	0 46 49.68	20 28 10.30	0.098	3	20.95	21.37	20.06	19.77	19.99	19.35	19.12	18.97	18.72	19.15	18.54	18.46	18.42	18.31	17.98
158	0 46 49.70	20 43 22.00	0.096	2	19.90	19.21	18.96	18.40	18.35	18.10	17.97	17.93	17.72	17.63	17.58	17.53	17.42	17.42	17.28
159	0 46 49.97	20 28 35.90	0.101	2	20.54	20.11	19.90	19.00	18.69	18.37	18.18	18.01	17.79	17.46	17.64	17.53	17.41	17.25	17.09
160	0 46 50.02	20 20 25.90	0.084	2	21.23	20.27	20.51	19.67	19.20	19.05	19.02	18.68	18.56	18.52	18.39	18.19	18.22	18.13	18.04
161	0 46 50.39	20 20 35.50	0.087	2	20.68	20.93	20.71	19.73	19.47	19.26	19.01	18.75	18.55	18.34	18.32	18.20	18.11	18.02	17.93
162	0 46 50.59	20 45 35.90	0.093	2	19.75	19.36	18.76	18.50	18.42	18.23	18.16	18.08	17.92	18.04	17.75	17.78	17.74	17.62	17.57
163	0 46 51.33	20 15 46.20	0.086	1	20.19	19.54	19.11	18.33	18.15	18.00	17.62	17.55	17.37	17.33	17.26	17.18	17.15	17.01	16.97
164	0 46 52.00	20 41 29.80	0.092	4	22.06	22.41	21.32	20.33	20.09	20.02	20.09	19.77	19.56	19.30	19.56	19.31	19.35	19.28	18.49

Table 3—Continued

No.	R.A.	Decl.	z_{ph}	T	a	b	c	d	e	f	g	h	i	j	k	m	n	o	p
165	0 46 52.98	20 21 48.00	0.105	1	20.79	20.53	20.40	19.46	19.45	19.37	19.21	19.21	19.04	19.38	19.04	19.06	19.04	18.98	18.59
166	0 46 53.04	20 29 39.20	0.110	3	21.74	23.59	24.08	21.51	21.35	21.12	21.96	20.80	20.49	21.17	21.20	20.48	20.77	20.16	19.43
167	0 46 53.08	20 29 54.80	0.106	1	21.71	22.18	21.01	20.67	20.40	20.26	20.09	20.35	19.92	19.47	19.91	20.14	20.11	19.39	19.10
168	0 46 55.60	20 34 34.60	0.092	1	22.10	20.75	20.41	19.89	19.21	18.91	18.76	18.57	18.39	18.22	18.23	18.08	17.95	17.89	17.81
169	0 46 55.88	20 28 44.80	0.094	1	20.85	19.29	19.46	18.41	17.89	17.61	17.42	17.22	17.01	16.94	16.83	16.71	16.58	16.45	16.36
170	0 46 57.48	20 28 37.60	0.100	2	21.35	21.20	20.28	19.46	19.06	18.77	18.65	18.36	18.18	18.03	17.90	17.90	17.79	17.54	17.40
171	0 46 58.32	20 37 57.80	0.089	1	20.42	19.97	19.79	19.40	19.45	19.25	19.13	19.16	19.14	19.08	19.13	19.02	19.08	19.18	18.80
172	0 47 05.18	20 38 27.40	0.090	1	20.19	19.26	19.38	18.33	17.85	17.59	17.40	17.21	17.00	16.93	16.80	16.71	16.60	16.48	16.43
173	0 47 13.04	20 35 34.20	0.110	3	21.05	20.14	20.63	19.75	19.41	19.07	18.99	18.74	18.54	18.30	18.39	18.29	18.24	17.90	18.05
174	0 47 14.30	20 33 10.00	0.090	1	21.15	20.97	21.04	19.60	19.49	19.42	19.15	19.14	18.97	18.94	18.76	18.84	18.77	18.67	18.53
175	0 47 14.44	20 17 55.70	0.087	1	20.04	19.67	19.23	18.40	18.18	18.13	17.84	17.71	17.59	17.48	17.45	17.43	17.38	17.31	17.14
176	0 47 15.15	20 37 12.40	0.090	1	20.79	20.24	19.94	19.37	19.13	18.90	18.86	18.75	18.64	18.29	18.33	18.39	18.21	18.31	17.95
177	0 47 15.19	20 17 54.90	0.100	2	20.68	20.63	20.96	19.92	19.57	19.09	18.91	18.67	18.51	18.08	18.34	18.23	18.11	17.98	17.70
178	0 47 15.45	20 26 06.40	0.087	7	20.75	21.19	20.46	20.36	20.32	20.04	20.12	19.85	19.47	20.03	19.59	19.74	20.13	20.49	18.85
179	0 47 15.49	20 37 46.60	0.112	3	23.64	22.49	22.85	21.11	20.96	21.07	20.95	20.99	20.20	20.05	20.03	20.96	21.37	19.35	19.60
180	0 47 15.73	20 37 06.90	0.096	1	21.01	19.80	19.58	18.52	18.18	17.89	17.70	17.53	17.31	17.14	17.08	17.05	16.92	16.78	16.67
181	0 47 15.78	20 36 02.70	0.105	2	20.93	20.34	21.09	20.66	19.60	19.41	19.28	18.91	18.73	18.50	18.80	18.53	18.40	18.22	18.13
182	0 47 16.11	20 37 00.10	0.097	3	20.86	20.99	20.14	19.34	19.01	18.71	18.59	18.37	18.21	17.79	17.94	17.87	17.75	17.58	17.49
183	0 47 16.39	20 24 44.60	0.092	1	19.97	19.15	18.96	18.11	17.70	17.26	17.03	16.93	16.72	16.60	16.62	16.38	16.34	16.21	16.10
184	0 47 19.13	20 38 03.90	0.096	1	20.32	19.47	19.52	18.59	18.32	18.00	17.74	17.62	17.41	17.34	17.18	17.13	16.99	16.83	16.84
185	0 47 20.07	20 20 33.60	0.095	1	21.69	21.19	20.46	20.40	20.48	20.07	20.32	20.17	19.99	19.61	19.78	19.98	20.17	20.23	19.51
186	0 47 20.25	20 37 59.50	0.100	3	20.41	19.77	19.65	18.98	18.75	18.55	18.46	18.23	18.00	18.02	17.73	17.77	17.65	17.54	17.34
187	0 47 22.08	20 33 14.50	0.110	5	20.02	19.70	19.51	19.10	19.08	18.87	18.85	18.79	18.75	18.60	18.65	18.61	18.66	18.46	18.46
188	0 47 25.93	20 33 08.50	0.090	2	20.58	20.57	20.00	19.33	19.17	19.09	18.81	18.63	18.46	18.51	18.56	18.47	18.44	18.32	18.13
189	0 47 26.79	20 29 36.40	0.106	3	19.88	19.39	19.44	18.48	18.35	18.24	18.06	18.00	17.81	17.73	17.63	17.67	17.52	17.39	17.39
190	0 47 26.90	20 29 40.40	0.101	4	19.68	19.29	19.20	18.39	18.25	18.10	17.94	17.83	17.65	17.58	17.37	17.41	17.27	17.09	17.16
191	0 47 27.72	20 28 00.60	0.094	1	20.43	19.70	19.72	18.65	18.41	18.12	17.97	17.75	17.58	17.32	17.39	17.30	17.19	17.08	17.00
192	0 47 28.08	20 27 54.10	0.097	2	19.36	18.61	18.64	17.71	17.37	17.15	16.93	16.78	16.55	16.46	16.37	16.30	16.16	16.03	15.94
193	0 47 28.38	20 27 49.60	0.094	1	19.79	19.06	18.99	18.08	17.72	17.50	17.27	17.16	16.92	16.80	16.72	16.67	16.54	16.38	16.38
194	0 47 35.16	20 34 40.90	0.086	5	19.85	19.62	19.36	18.88	18.85	18.79	18.67	18.72	18.48	18.61	18.43	18.31	18.21	18.34	18.17
195	0 47 36.48	20 33 34.30	0.108	1	21.21	21.15	21.02	20.13	19.56	19.20	18.96	18.71	18.41	18.43	18.17	18.09	17.87	17.72	17.50
196	0 47 39.75	20 35 57.10	0.083	1	19.32	18.46	18.43	18.11	18.00	17.96	17.88	17.86	17.80	17.84	17.72	17.78	17.83	17.77	17.62
197	0 47 40.64	20 33 36.70	0.087	1	19.59	18.94	18.70	18.17	17.98	17.95	17.77	17.70	17.53	17.36	17.41	17.35	17.33	17.29	17.26
198	0 47 43.38	20 32 35.00	0.090	1	20.46	20.04	19.71	19.23	18.87	18.87	18.78	18.61	18.49	17.94	18.31	18.33	18.28	18.23	18.08